Numerical Modeling of Concrete Microstructure with Poly-mineral Aggregate using Image-based Analysis

<u>Hyeong-Tae Kim</u>, PhD

Kyoungsoo Partk, PhD

Computational & Experimental Mechanics Group
School of Civil & Environmental Engineering
Yonsei University, Seoul, Korea

November 6, 2023

Motivation

Concrete degradation by neutron

Shin Kori, Nuclear Power Plants, IAEA Image bank

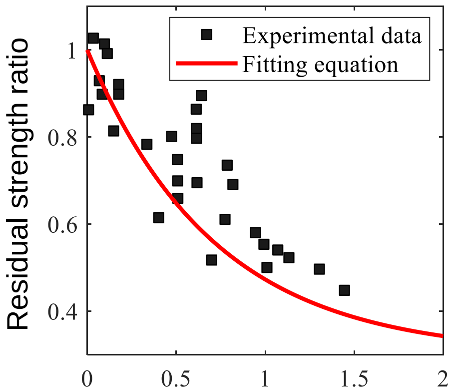

Linear expansion of concrete (%)

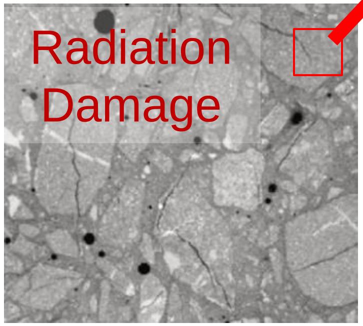

Swiss Federal Laboratories for Material Testing and Research

Radiation effects on the aggregate

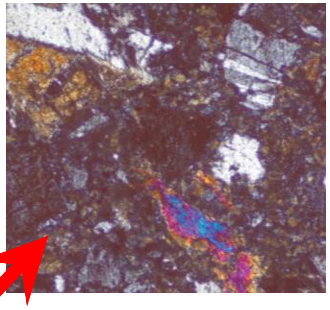

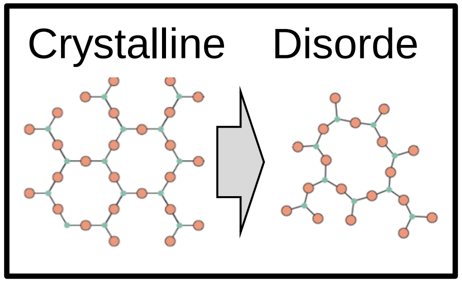

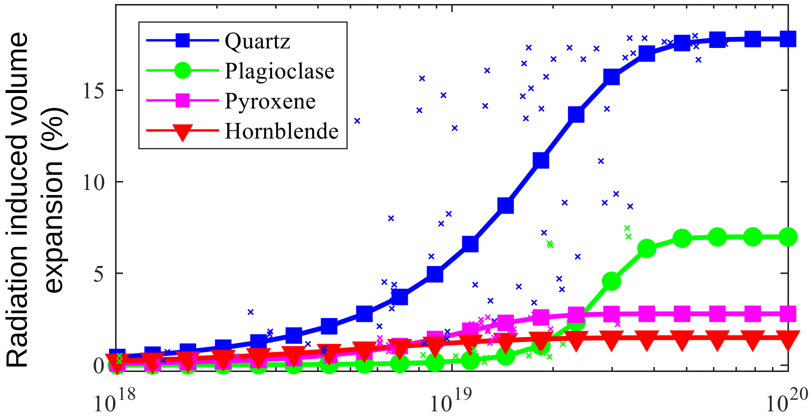

Fluence of neutron radiation (n/cm^2)

- Maruyama, I., Kontani, O.,Takizawa, M., Sawada, S.,Ishikawao, S., Yasukouchi, J., ... & Igari, T. (2017). Development of soundness assessment procedure for concrete members affected by neutron and gamma-ray irradiation. *Journal of Advanced Concrete Technology*, *15*(9), 440-523.
- Le Pape, Y., Alsaid, M. H., & Giorla, A. B. (2018). Rock-forming minerals radiation-induced volumetric expansion–revisiting literature data. Journal of Advanced Concrete Technology, 16(5), 191-209.

Contents

Image Acquisition

◻ Concrete Specimen

■ Mixing Design

Mix component		Density (kg/m³)	Volume (m³)
Portland Cement [CEM I 42.5 R]		3.1	137.1
Water		1	166.0
Aggregate	Quartz [석영] 0~2 mm	2.65	198.1
	Gabbro [반려암] 2~8 mm	2.94	448.0
Admixture	Plasticizer	1.04	2.8
	Air entraining agent	1.05	0.7

■ Size

- ◻ Specimen : 20 x 20 x 80 mm (Cut)

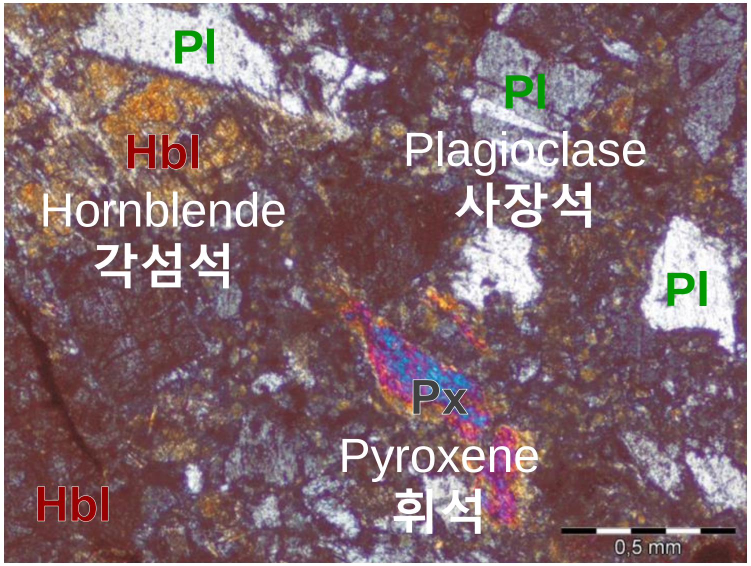

- Dąbrowski, M., Glinicki, M. A., Dziedzic, K., & Antolik, A. (2019). Validation of sequential pressure method for evaluation of the content of microvoids in air entrained concrete. Construction and Building Materials, 227, 116633.
- Jóźwiak-Niedźwiedzka, D., Antolik, A., Dziedzic, K., Glinicki, M. A., & Gibas, K. (2019). Resistance of selected aggregates from igneous rocks to alkali-silica reaction: verification. *Roads and Bridges-Drogi i Mosty*, *18*(1), 67-83.

Image Segmentation

□ X-ray CT (Depend on the material density)

Image Segmentation : Otsu method

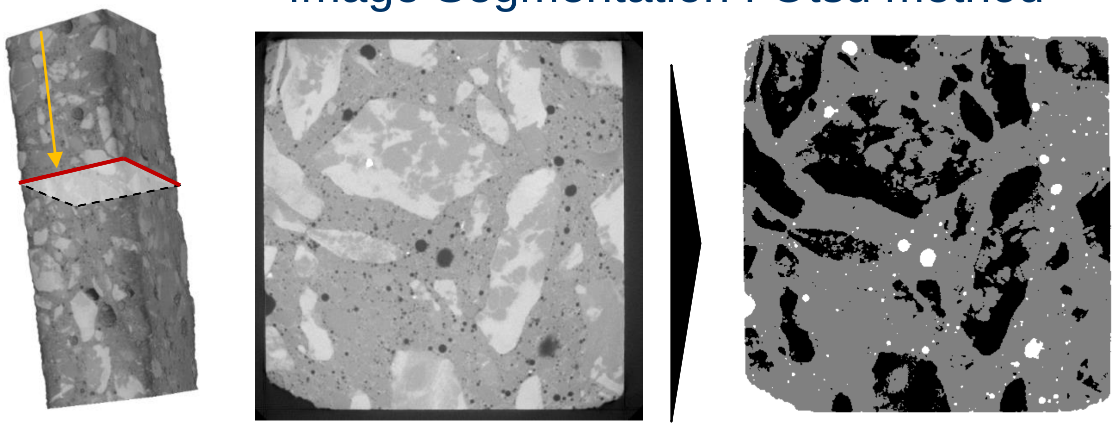

ρ_{Quartz} = 2.67 g/cm^3
(Howie et al. 1992)

ρ_{C-S-H} = 2.604 g/cm^3
(Allen et al. 2007)

□ Neutron CT (Depend on the hydrogen components)

Image Segmentation : Otsu method

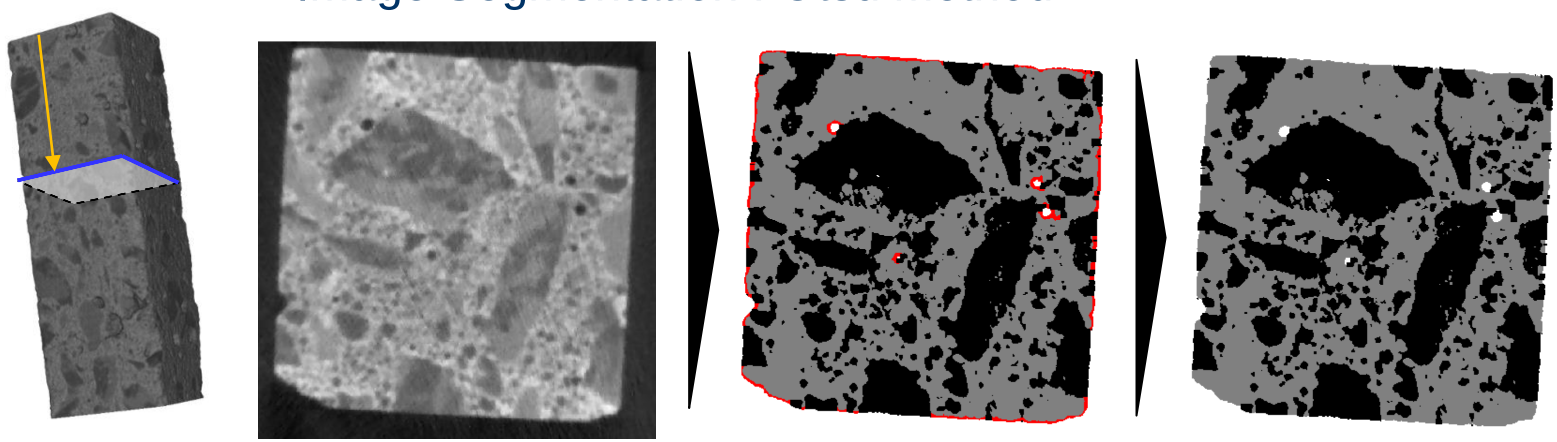

Microstructure Reconstruction

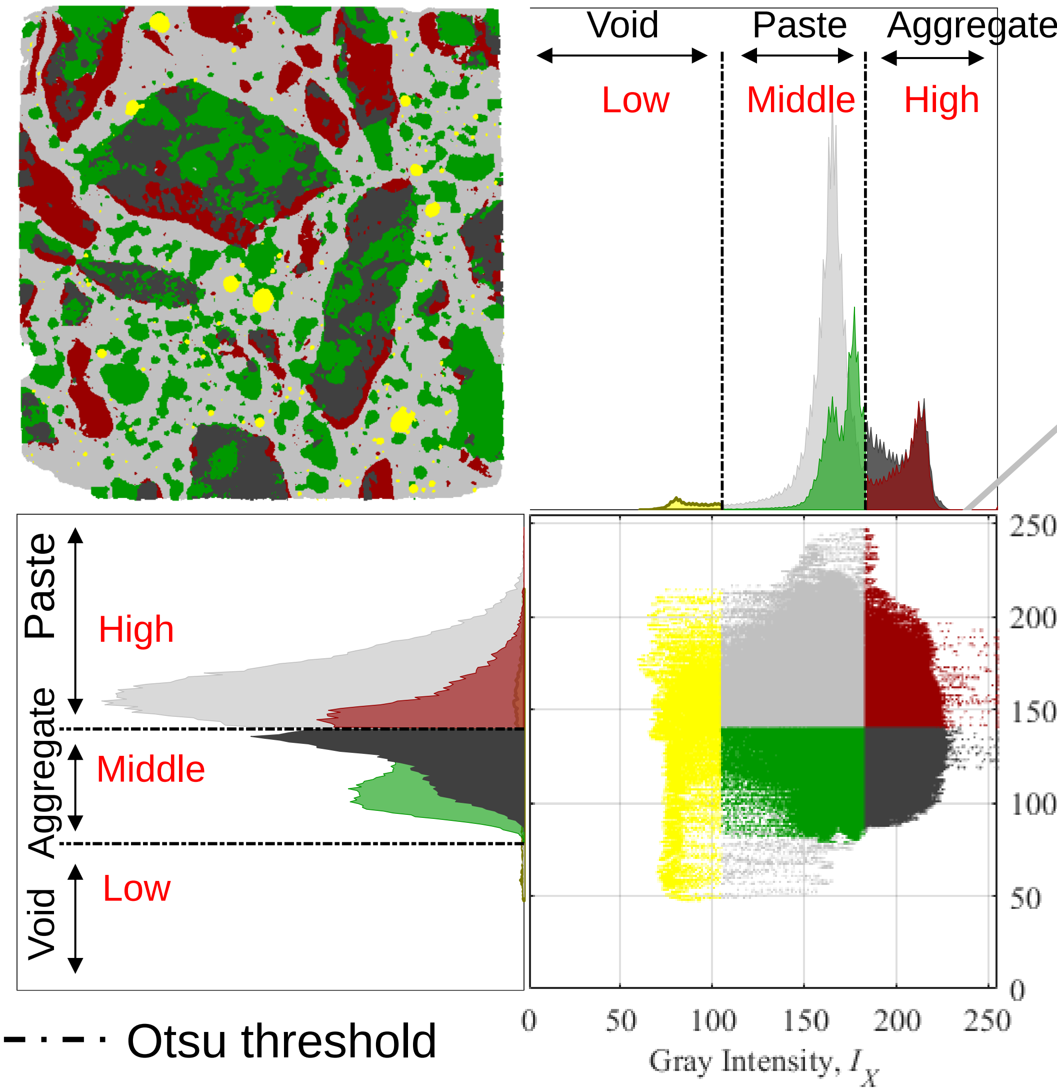

- Void
- Paste
- Aggregate (X-ray only)
- Aggregate (Neutron only)
- Aggregate (X-ray and neutron)

C-S-H (Paste)
$[(CaO)_3(SiO_2)_2(H_2O)_3, \approx 2.60\ g/cm^2]$

Hornblend [각섬석](Gabbro)
$[(Ca, Na)_{2\sim3}(Mg, Fe, Al)_5(Al, Si)_8O_{22}(OH, F)_2, \approx 3.31\ g/cm^2]$

Plagioclase [사장석] (Gabbro)
$[(Ca, Na)Al_2Si_2O_8, \approx 2.67\ g/cm^2]$
Quartz [석영] (sand)
$[SiO_2, \approx 2.65\ g/cm^2]$

Pyroxene [휘석] (Gabbro)
$[(Mg, Fe)_2Si_2O_6, \approx 3.58\ g/cm^2]$

H.T. Kim, D.F.T. Razakamandimby, V. Szilagyi, K. Zoltan, L. Szentmiklosi, M.A. Glinicki, and K. Park, 2021 Reconstruction of concrete microstructure using complementarity of X-ray and neutron tomography, Cement and Concrete Research 148, 106540

Microstructure Reconstruction

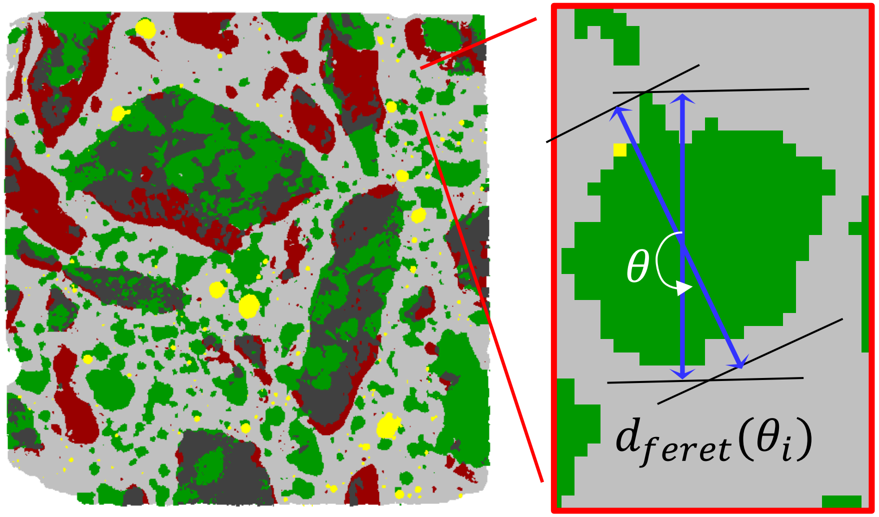

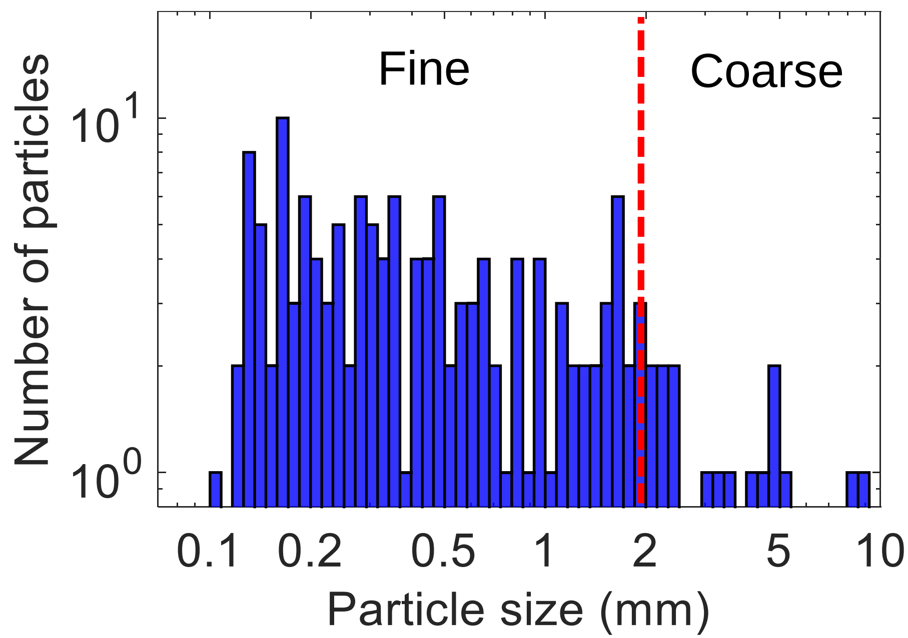

Particle size = $\frac{1}{180}\sum_{i=1}^{180} d_{feret}(\theta_i)$

Quartz [석영]

1. Pure mineral particle
2. Particle size = 0~2mm

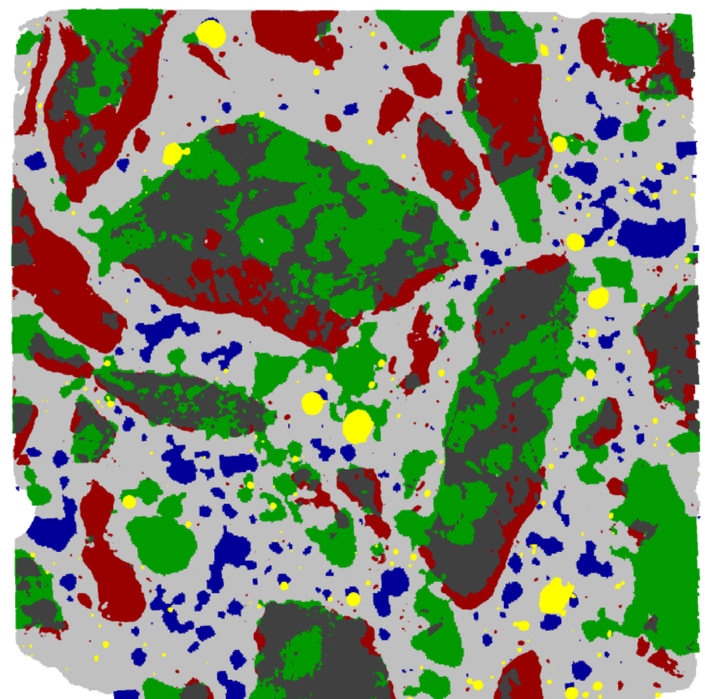

Mesh Generation Based on the Image

Homogeneous Mesh

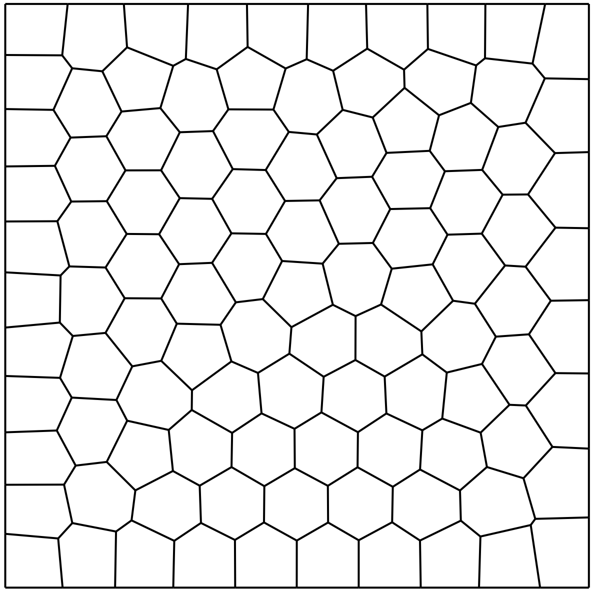

# of elements = 100

# of nodes = 202

Microstructure Mesh

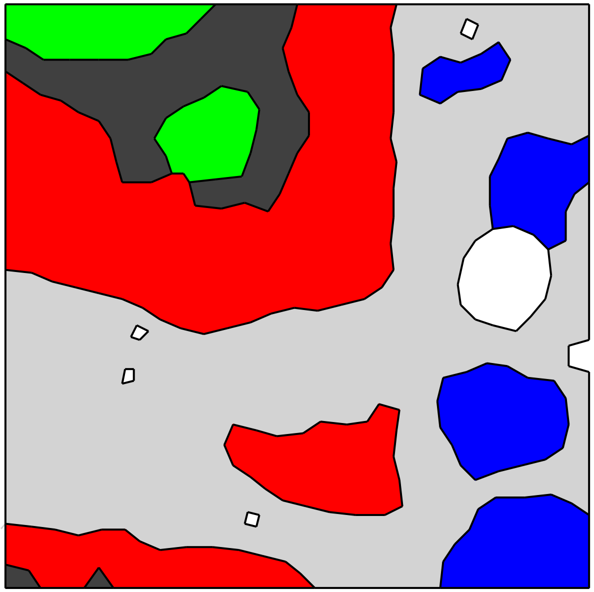

# of elements = 13

# of nodes = 210

Polygonal Mesh

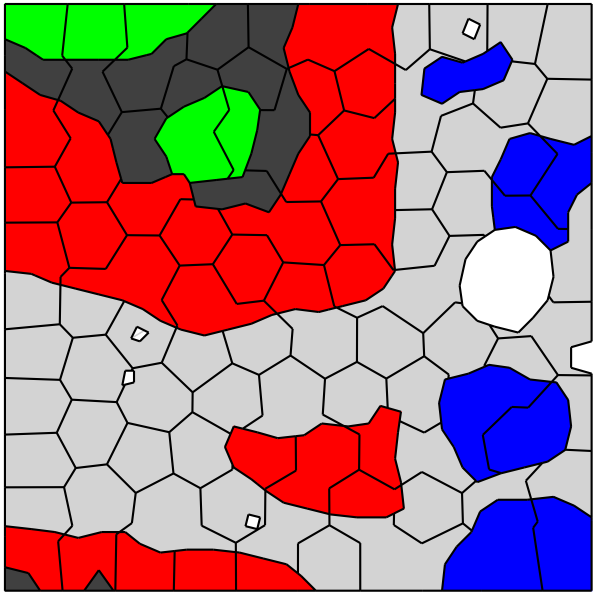

# of elements = 100

# of nodes = 464

- **<u>Kim, H. T., & Park, K</u>**. 2022. Computed Tomography (CT) Image-based Analysis of Concrete Microstructure using Virtual Element Method. *Composite Structures*, 115937.
- Talischi, C., Paulino, G. H., Pereira, A., & Menezes, I. F. M. (2012). PolyMesher: A general-purpose mesh generator for polygonal elements written in Matlab. Structural and Multidisciplinary Optimization, 45(3), 309–328

Microstructure Mesh Generation

- Microstructure acquisition

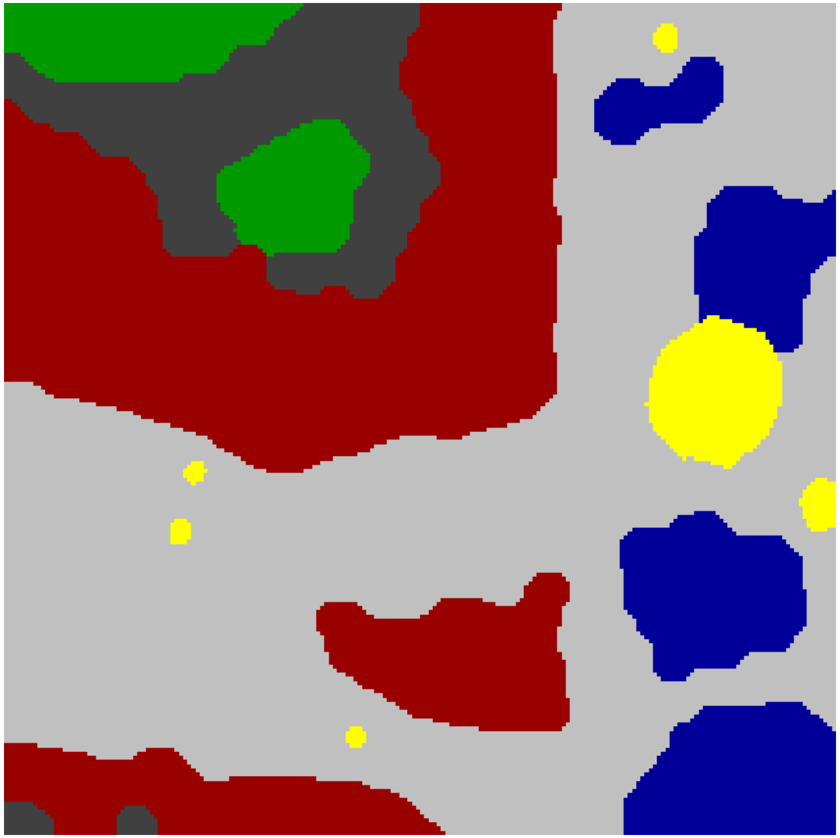

200 × 200 pixel , Poly-mineral

- Edge Detection

Edge Type : Combination of Material

Microstructure Mesh Generation

- Node Positioning (coarsening)

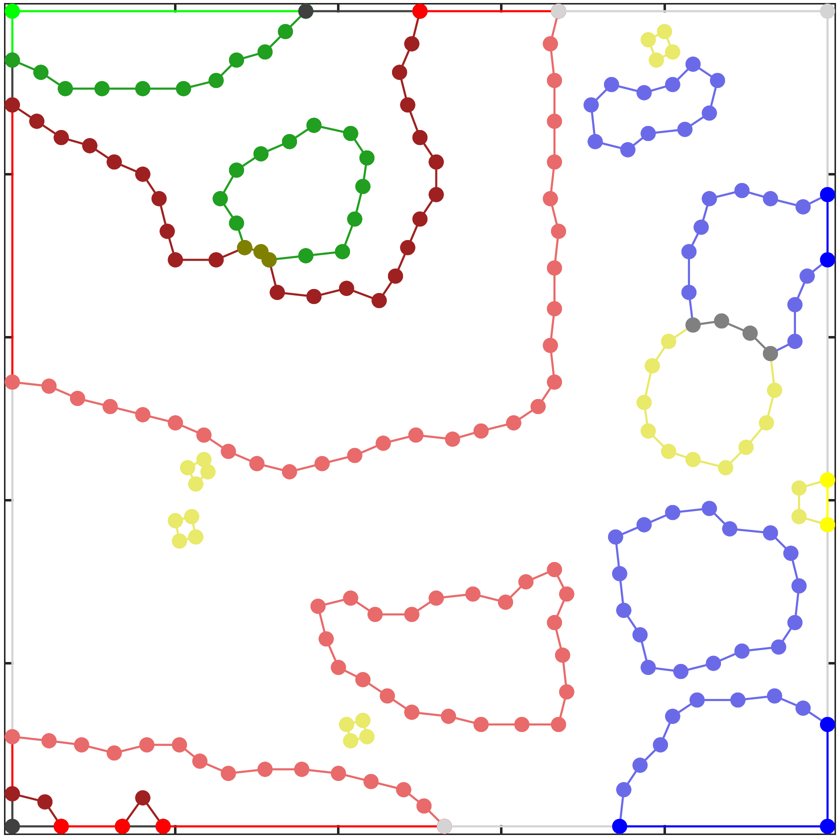

node space = Characteristic edge length $[l_{e,ch}]$

- Mesh Generation

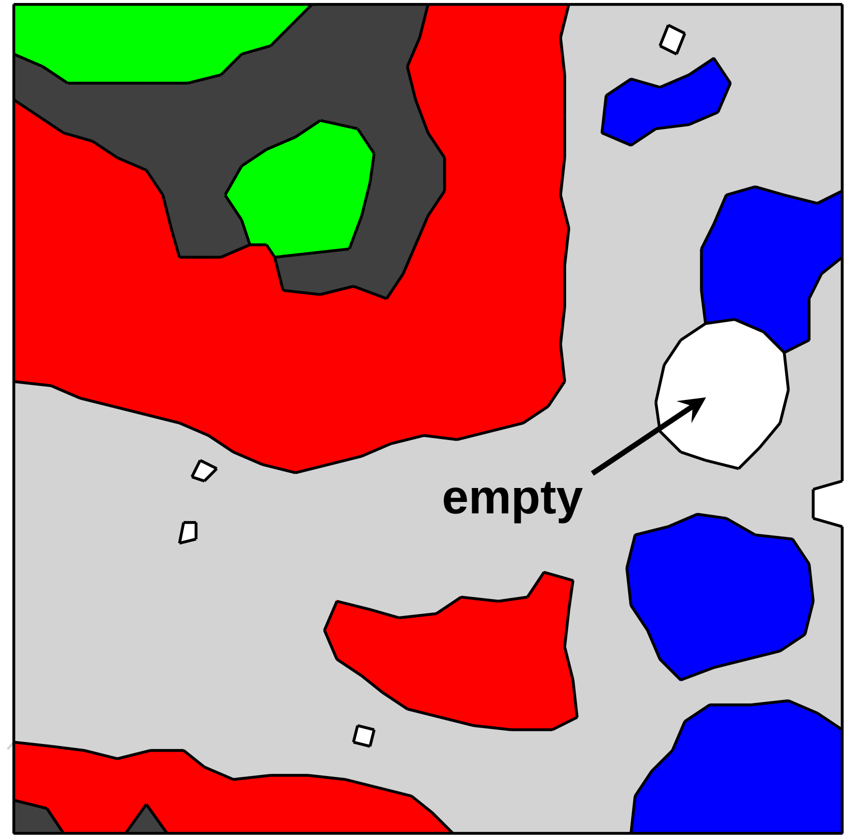

Except void particles

Polygonal Mesh Generation

▫ Integration with Microstructure and Homogeneous Mesh

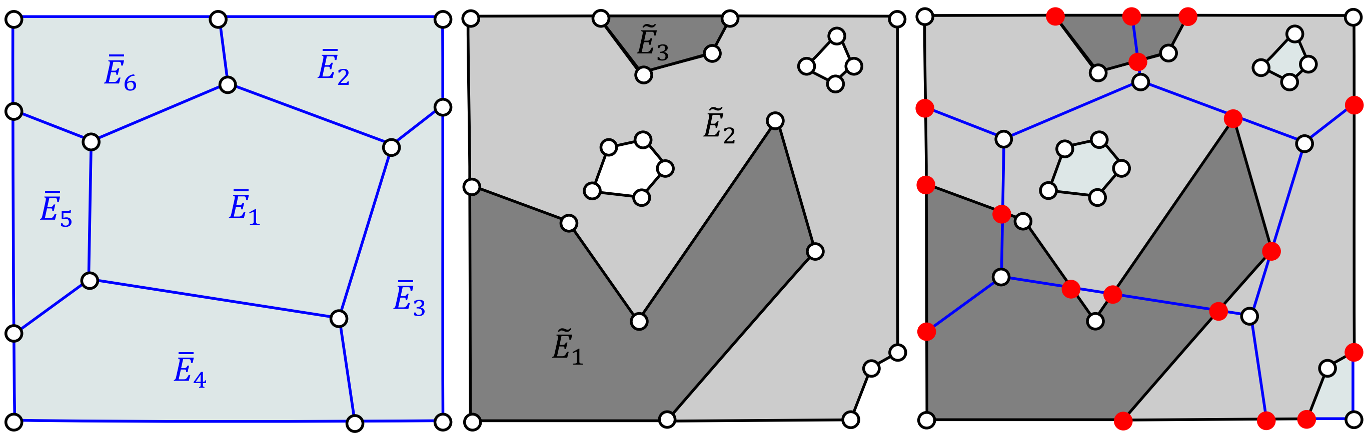

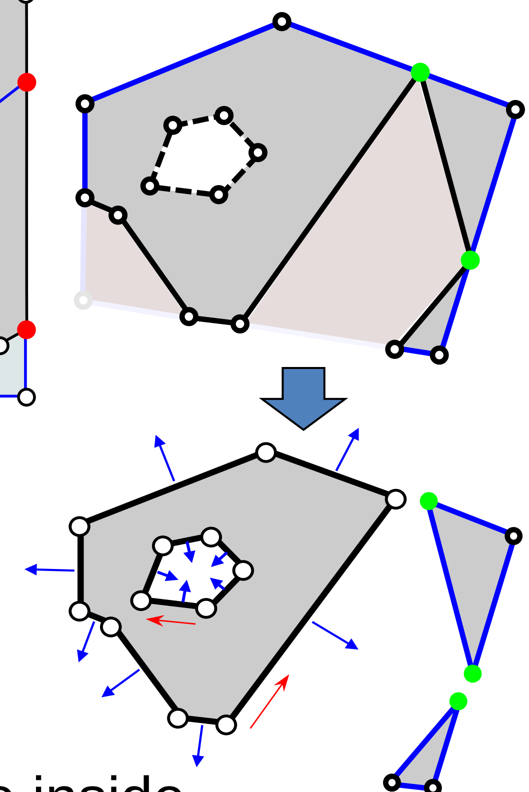

1. Create the intersection nodes
2. Split the edges by new nodes
3. Divided the elements based on the mesh data
4. Check the element positing – assemble the hole inside

- **<u>Kim, H. T., & Park, K</u>**. 2022. Computed Tomography (CT) Image-based Analysis of Concrete Microstructure using Virtual Element Method. *Composite Structures*, 115937.

Numerical Examples

$17.0016\ mm$

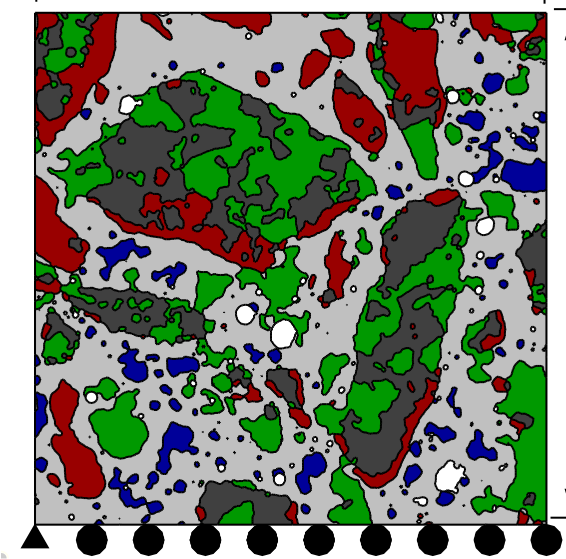

$17.0016\ mm$

$t = 1mm$

Domain size : 1232 x 1232 pixels

Radiation : $10^{18} \sim 2 \times 10^{21}\ n/cm^2$

Plane strain condition

Initial strain : $\boldsymbol{\varepsilon_{in}} = [\varepsilon_V/2 \quad \varepsilon_V/2 \quad 0]^T$

Aggregate Type

: poly-mineral vs homogeneous

$$a_{homogeneous} = \sum \frac{V_i}{V_{homogeneous}} a_i$$

	석영(Qz)	사장석(Pl)	휘석(Px)	각람석(hbl)	골재(Homo)	페이스트(Paste)
E(MPa)	94.73	94.90	88.94	141.14	104.93	20.00
v	0.0869	0.2786	0.3489	0.2424	0.2392	0.2000

Radiation Induced Volume Expansion

Fitting equation : Zubov and Ivanov'S sigmoidal model with linear temperature

$$\varepsilon_V(\Phi, T) = \varepsilon_{max} \frac{1 - e^{-\frac{\Phi}{\Phi_c}}}{1 + e^{-\frac{\Phi - \Phi_L}{\Phi_c}}}$$

characteristic fluence [Φ_c , n/pm^2]
Latency fluence [$\Phi_L, n/pm^2$]

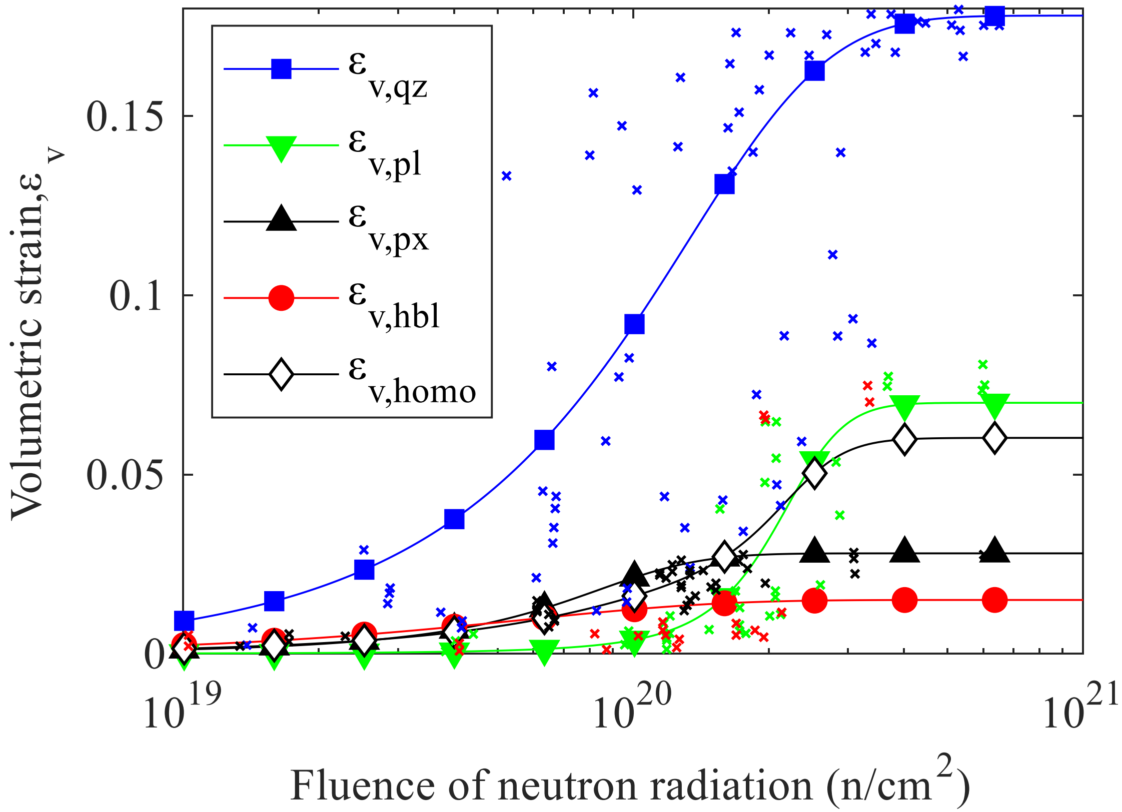

	ε_{max}(%)
석영[qz]	17.8
사장석[Pl]	7.0
휘석[Px]	2.8
각람석[Hbl]	1.5
골재[Homo]	6.0

[1] Le Pape, Y., Alsaid, M. H., & Giorla, A. B. (2018). Rock-forming minerals radiation-induced volumetric expansion–revisiting literature data. Journal of Advanced Concrete Technology, 16(5), 191-209.

Result

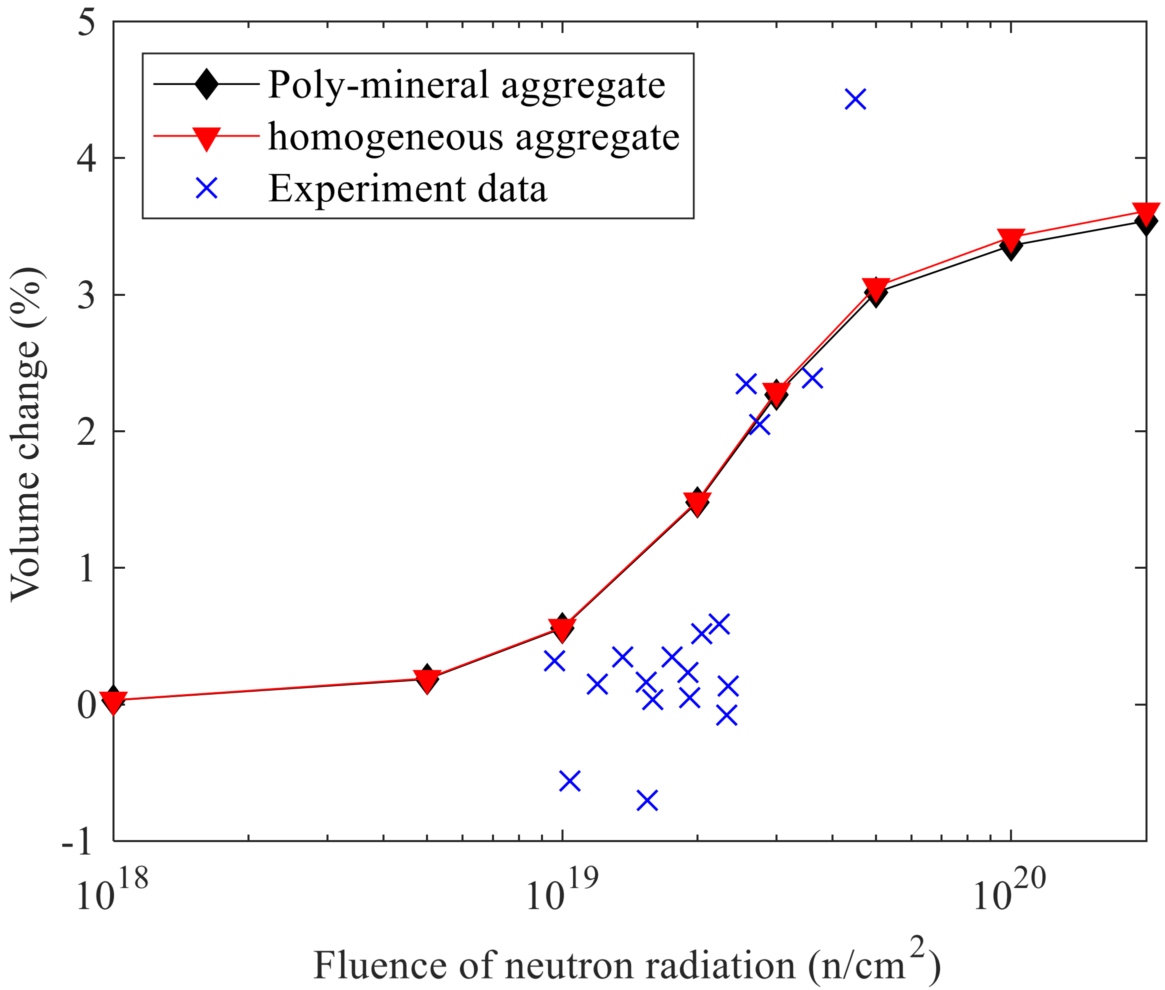

$$Volume\ change = \left|\frac{V - V_0}{V_0}\right|$$

$$V = \sum_{i=1}^{Nelem} A_i t$$

$$V_0 = \sum_{i=1}^{Nelem} A_{0,i} t$$

[1] Jing, Y., & Xi, Y. (2017). Theoretical Modeling of the Effects of Neutron Irradiation on Properties of Concrete. *Journal of Engineering Mechanics*, *143*(12), 04017137.

Result

Maximum Principal Strain

Radiation = $5 \times 10^{20}\ n/cm^2$

Homogeneous

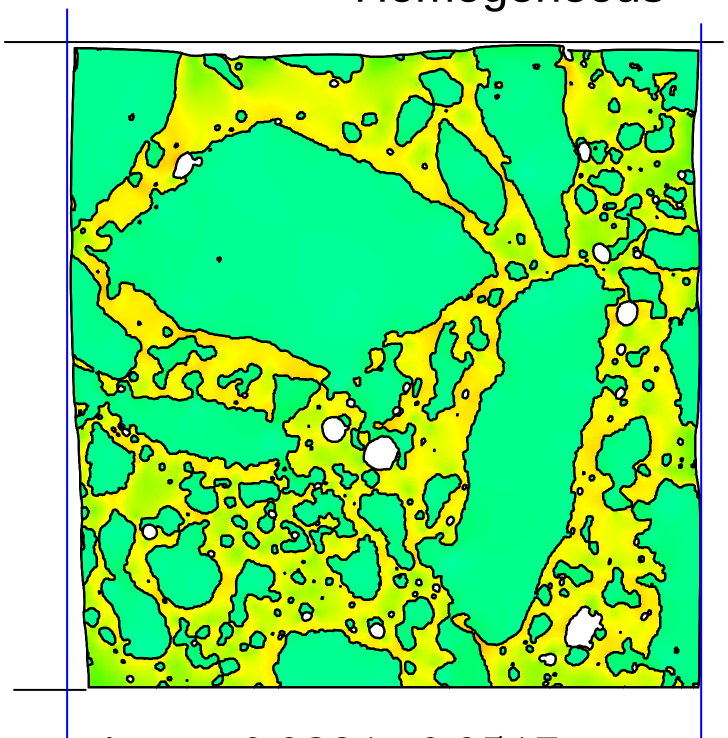

$\Delta\varepsilon = -0.0291 \sim 0.0517$

Poly-mineral

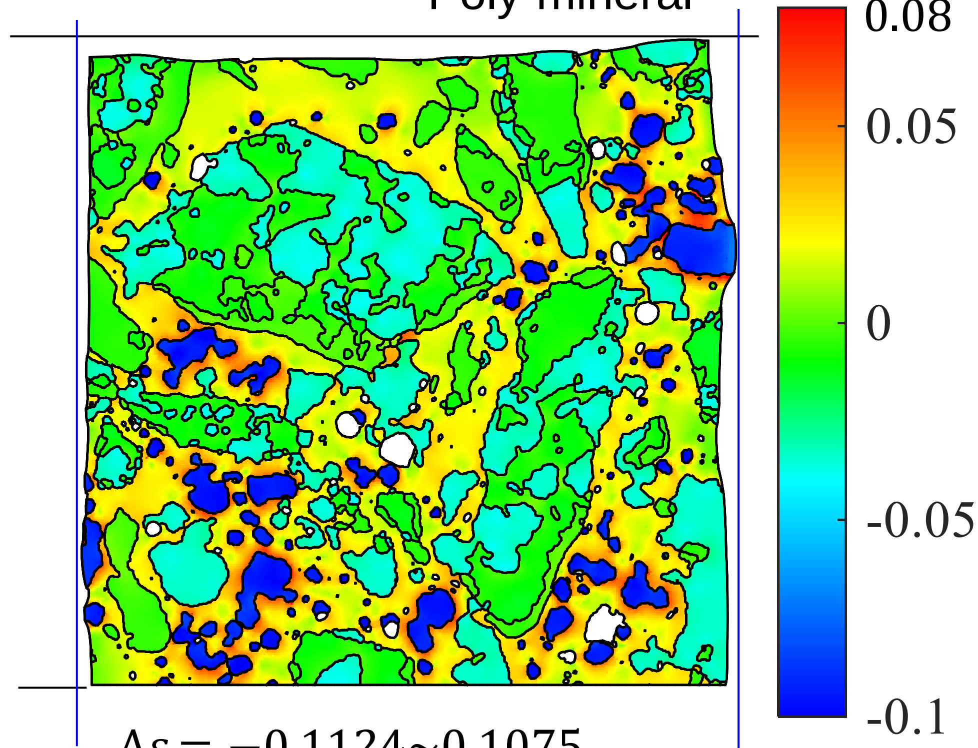

$\Delta\varepsilon = -0.1124 \sim 0.1075$

(Scale factor = 5)

Summary

- X-ray와 Neutron CT의 상호보완성과 mineral들의 특성을 이용하면 미세구조 내부의 mineral들의 분포에 대해 판별이 가능하다.
- 제안한 수치해석 모델 방법을 사용해 이미지만을 이용하여 복잡한 구조에 대해 다각형 요소로 해석에 요구되는 정확도 수준에 따른 이산화가 가능하다.
- 수치해석을 통해 얻은 중성자 조사량에 따른 콘크리트 팽창은 실험데이터와 유사한 경향성을 보인다.
- 골재에 대해 각 mineral별로 구분하여 해석을 수행한 결과는 homogeneous로 가정한 경우에 비해서 전체 부피 팽창률은 거의 동일한 결과를 보이지만 국부적인 영역에서 발생하는 변형과 예측되는 손상에 있어서 큰 차이를 나타낸다.

Question and Answer

Thank you

Rock-forming Minerals on the Aggregate

- Fine Aggregate : Quartz Sand [Quartz ≅ 98%]
- Coarse Aggregate : Gabbro [Plagioclase, Pyroxene, Olivine, Hornblende]

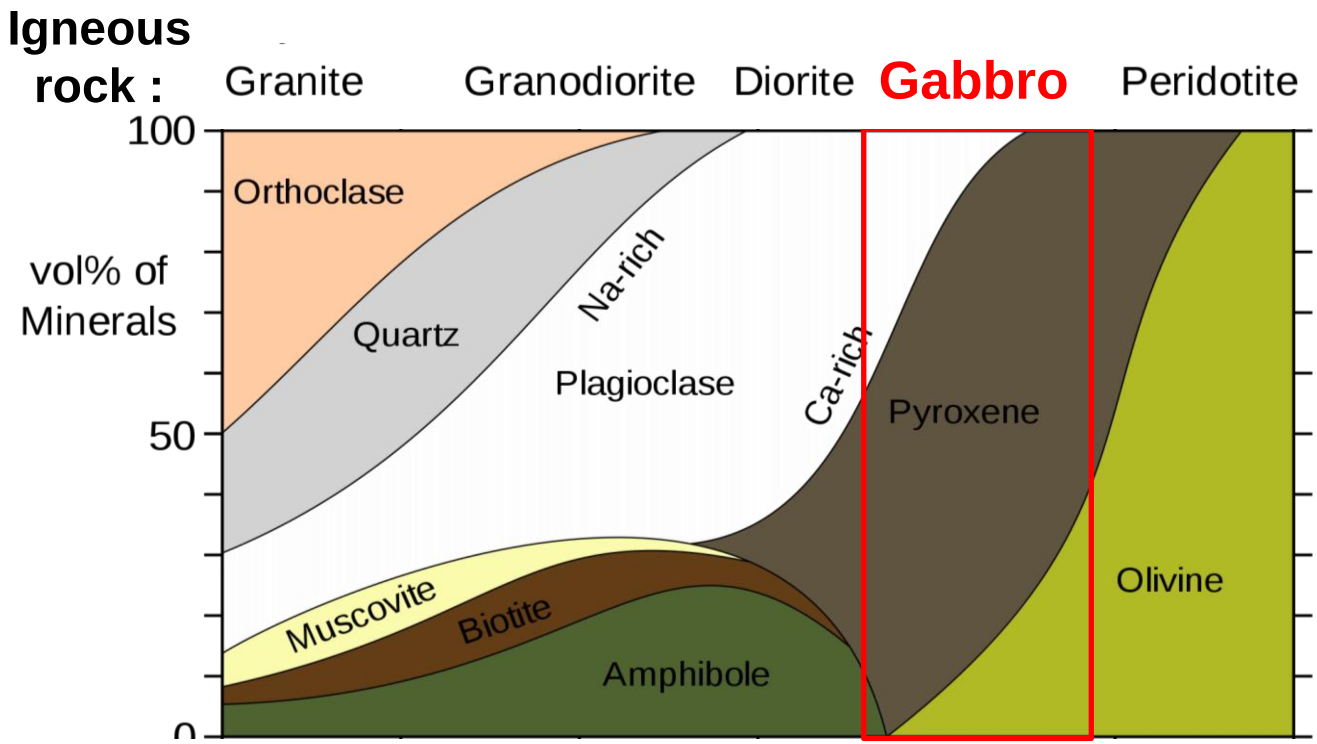

- Allaby, Michael (2013). "gabbro". *A dictionary of geology and earth sciences* (Fourth ed.). Oxford: Oxford University Press
- Dąbrowski, M., Glinicki, M. A., Dziedzic, K., & Antolik, A. (2019). Validation of sequential pressure method for evaluation of the content of microvoids in air entrained concrete. Construction and Building Materials, 227, 116633.

3D Concrete Microstructure

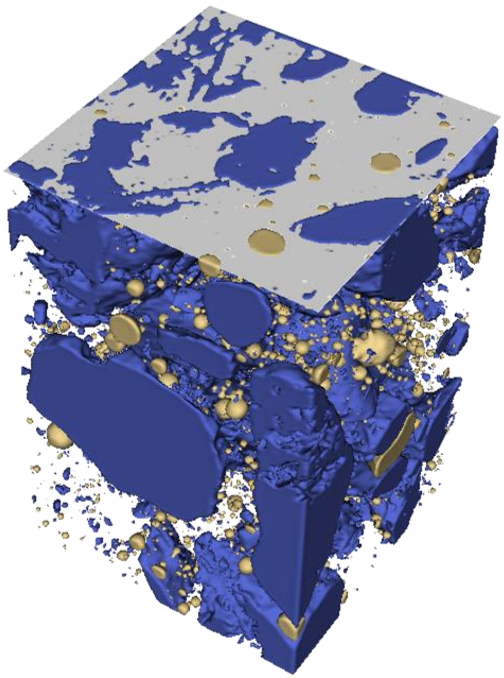

X-ray CT

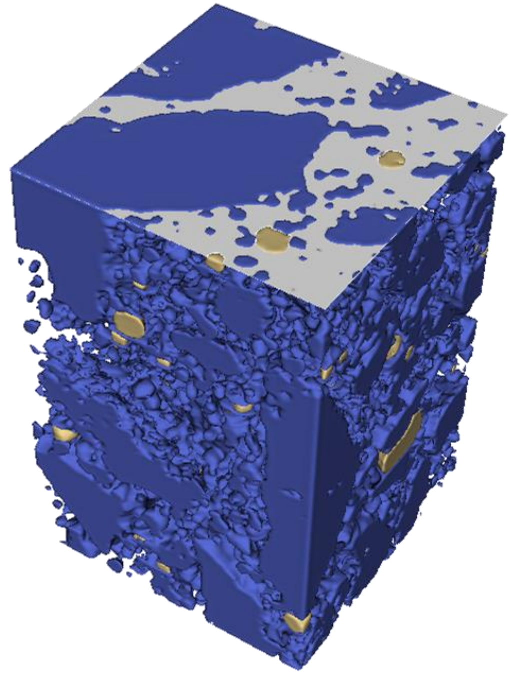

Neutron CT

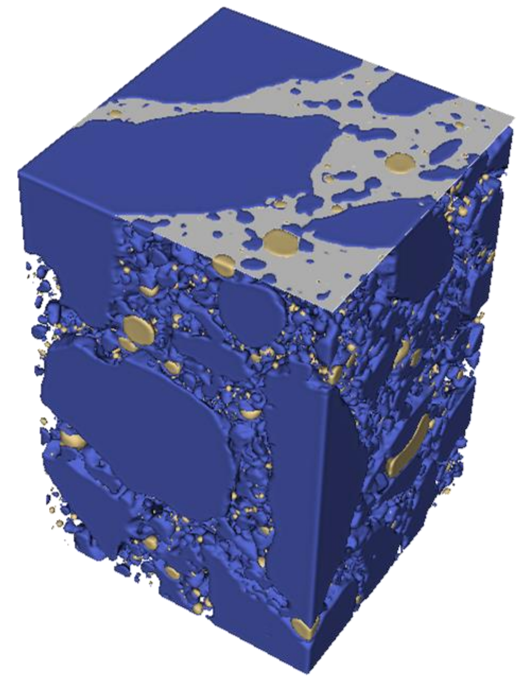

Assemble

H.T. Kim, D.F.T. Razakamandimby, V. Szilagyi, K. Zoltan, L. Szentmiklosi, M.A. Glinicki, and K. Park, 2021
Reconstruction of concrete microstructure using complementarity of X-ray and neutron tomography,
Cement and Concrete Research 148, 106540

Combined x-ray & neutron image

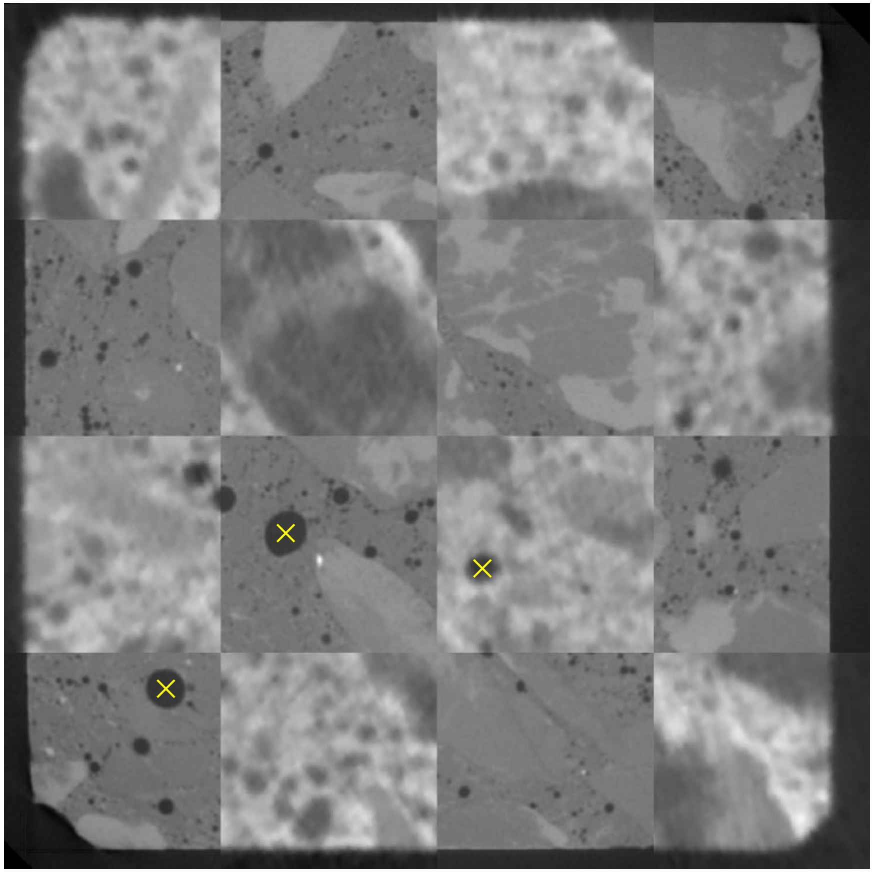

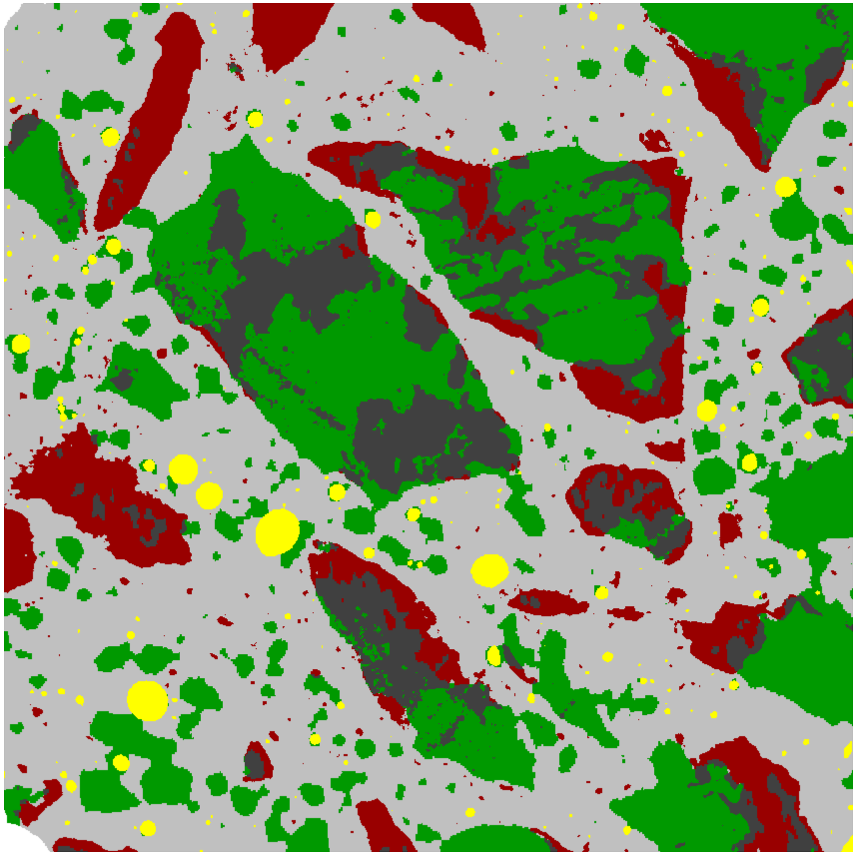

Morphological Filtering

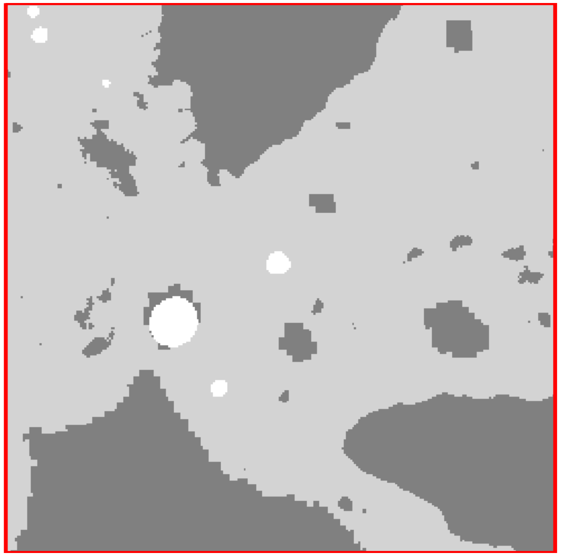

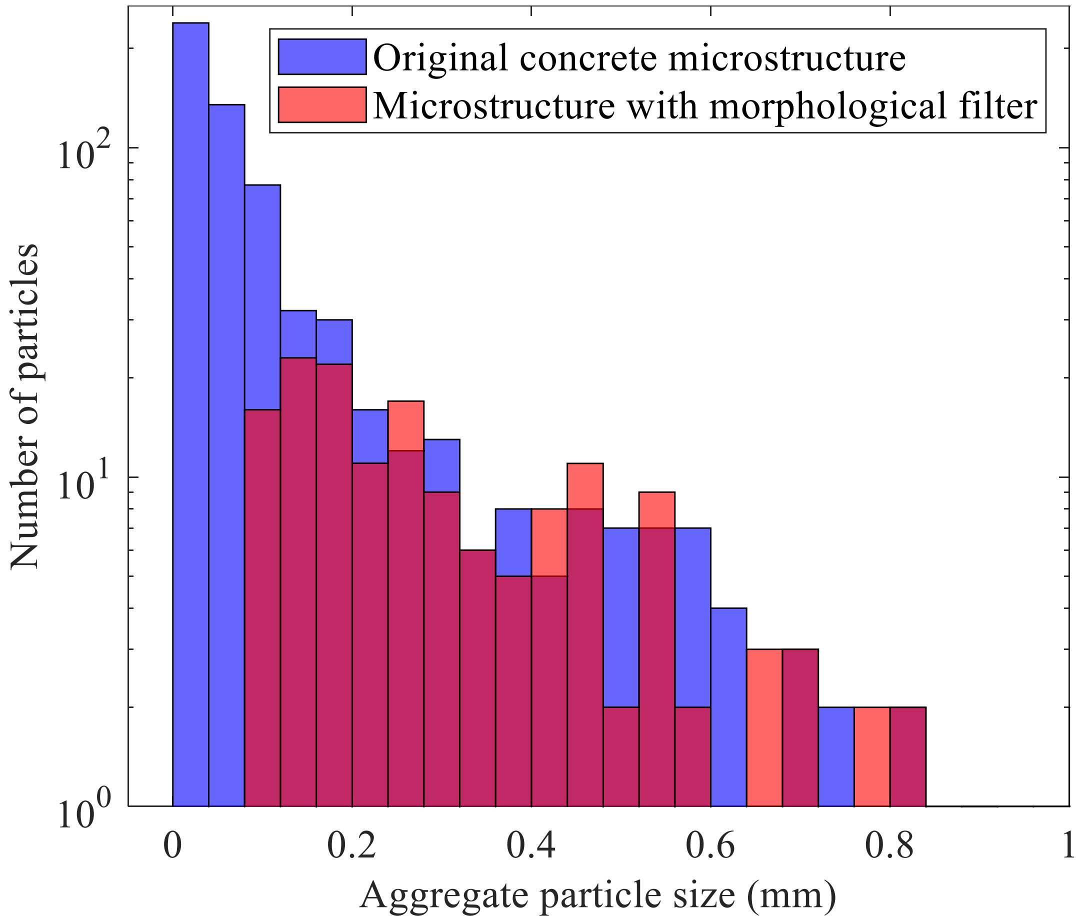

Verification

◻ Microstructure

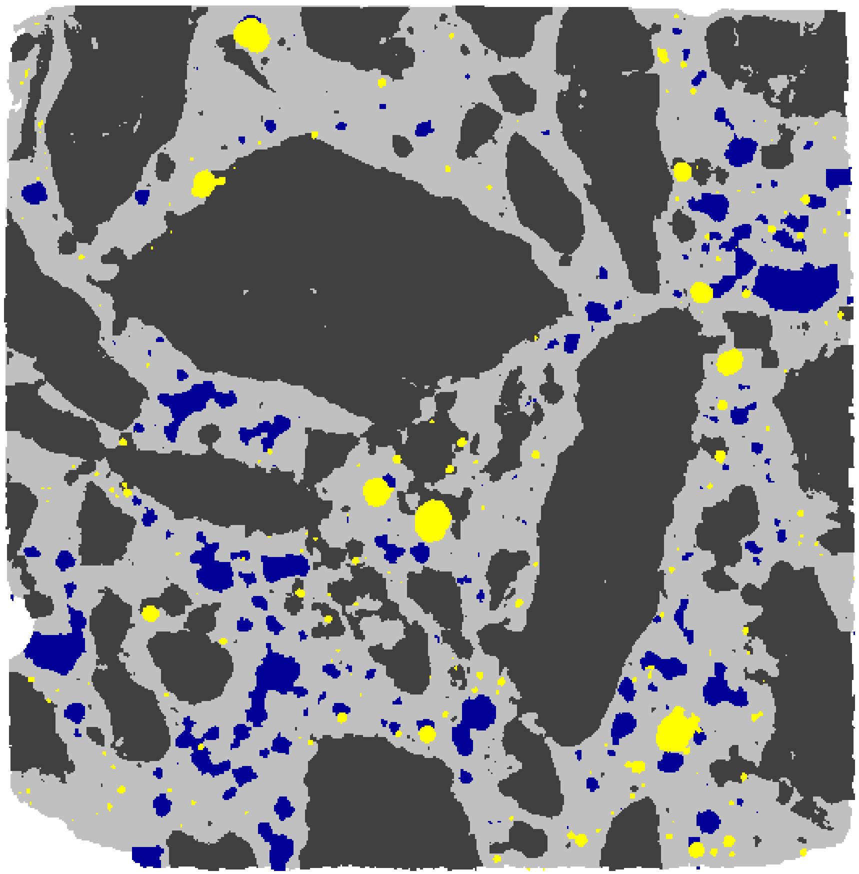

◻ Volume Fraction

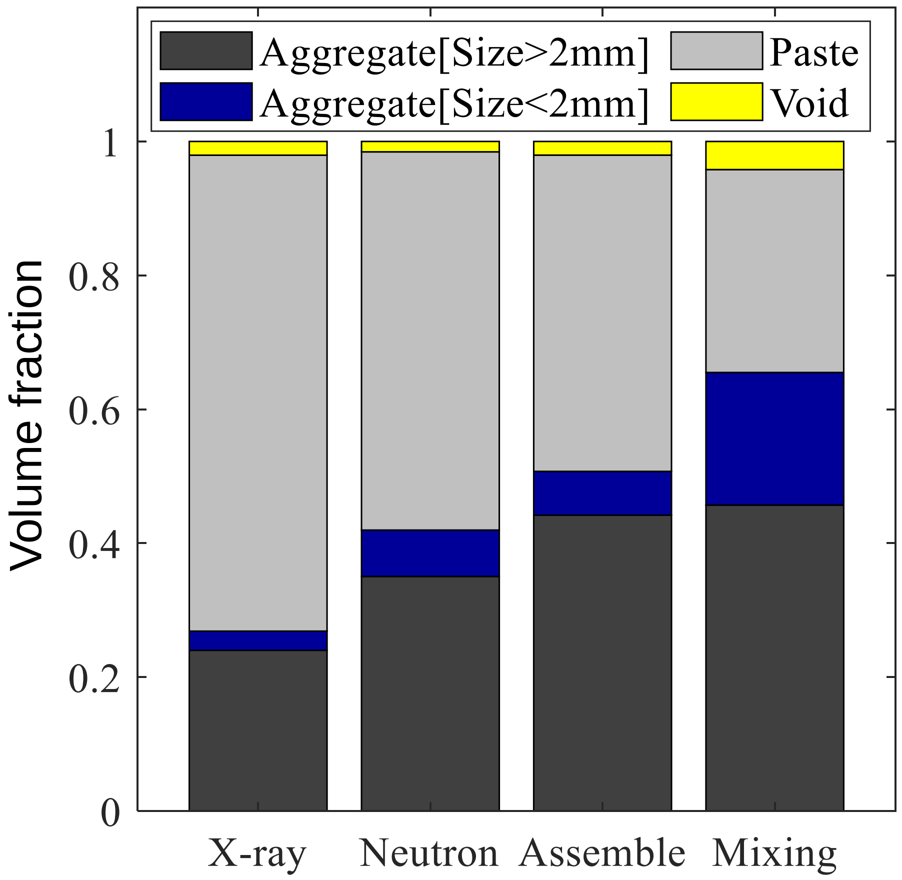

61 slides (10mm ~70mm)

Mesh Generation based on the Image

Microstructure

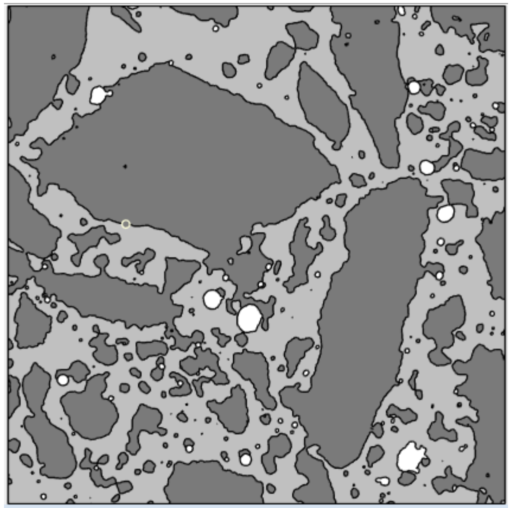

Centroidal Voronoi Tessellation (CVT)

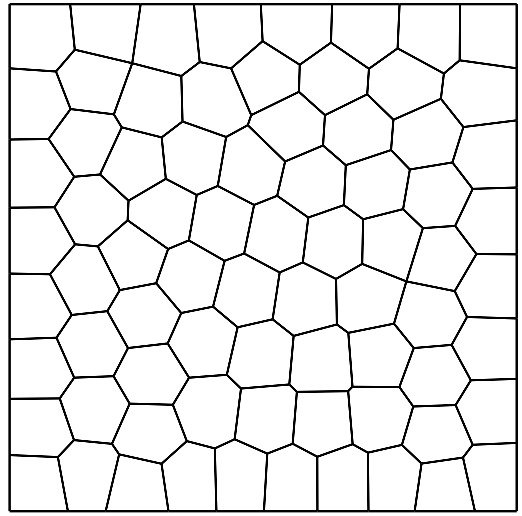

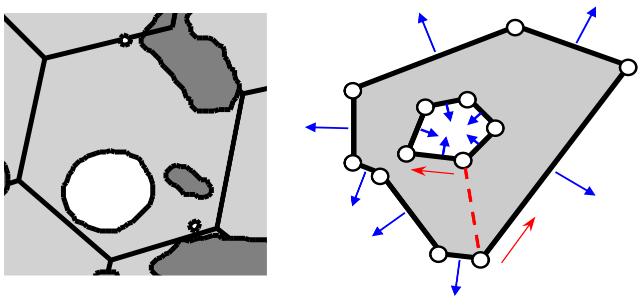

Non-simple Element

n_{elem} of CVT = 75

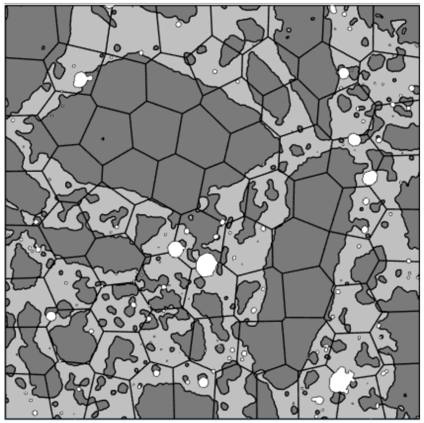

n_{elem} = 264

n_{elem} of CVT = 300

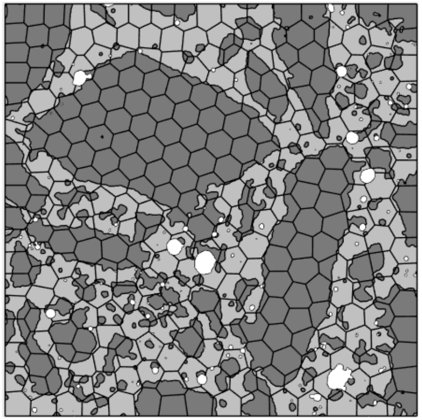

n_{elem} = 432

n_{elem} of CVT = 2500

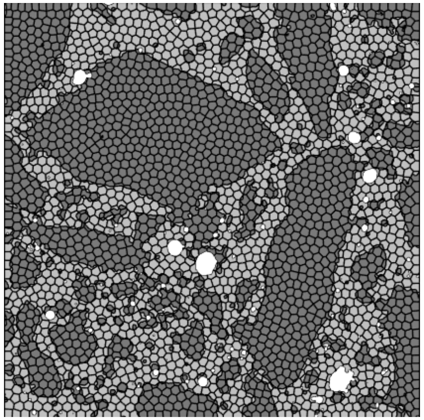

n_{elem} = 2497

n_{elem} of CVT = 10000

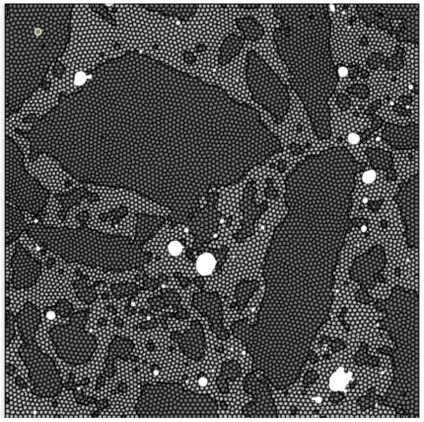

n_{elem} = 8956

Kim, H. T., & Park, K. 2022. Computed Tomography (CT) Image-based Analysis of Concrete Microstructure using Virtual Element Method. *Composite Structures*, 115937.

Virtual Element Formulation

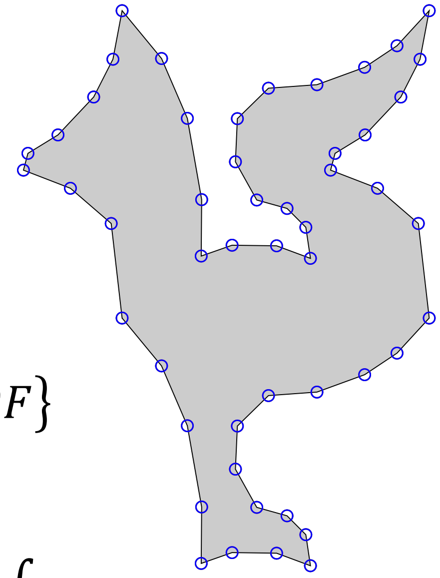

- **Governing Equation**

$$\int_{\Omega} \boldsymbol{\epsilon}(\boldsymbol{u}) : \boldsymbol{\sigma}(\mathbf{v})\, d\mathbf{x} = \int_{\partial\Omega} \mathbf{v} \cdot \mathbf{t}\ d\mathbf{x} \quad \forall \mathbf{v} \in \mathcal{K}_0$$

- **Preliminary Space**

$$\widetilde{\mathcal{V}}(F) = \{ v_h \in \mathcal{H}^1(F) : \Delta v_h \in \mathcal{P}_1(F) \text{ in } F, v_{h|e} \in \mathcal{P}_1(e)\ \forall e \in \partial F \}$$

- **First Projection by Projection Operator**

$$\int_E \Pi^0 \nabla \phi_i \cdot \mathbf{m}_\alpha\, d\mathbf{x} = \sum S_{i\beta} \int_E \mathbf{m}_\beta \cdot \mathbf{m}_\alpha d\mathbf{x} = \int_{\partial E} \phi_i \mathbf{m}_i \cdot \mathbf{n}\, d\mathbf{s} - \int_E \phi_i \mathrm{div} \mathbf{m}_i d\mathbf{x}$$

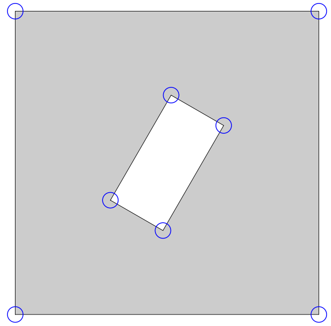

- **Projection of Displacement**

$$\int_E (\Pi^0 v_h) p\, d\mathbf{x} = \int_E v_h p\, d\mathbf{x} \quad \forall p \in \mathcal{P}(E)$$

$$p = \sum a_i \cdot m_i \quad m_1 = 1,\ m_2 = \left(\frac{x - x_c}{h_e}\right), m_3 = \left(\frac{y - y_c}{h_e}\right)$$

Beirão da Veiga, L., Brezzi, F., Cangiani, A., Manzini, G., Marini, L. D., & Russo, A, 2013, Basic principles of virtual element methods. *Mathematical Models and Methods in Applied Sciences*, 23(1), 199-214.

L^2 Projection Operator

◻ Projection of Displacement

$$\int_E (\Pi_1^0 v_h) p_1 \, d\mathbf{x} = \int_E v_h p_1 \, d\mathbf{x} \quad \forall p_1 \in \mathcal{P}_1(E)$$

$$p_1 = \sum_{\alpha=1}^{n_{p_1}} \alpha_\alpha m_\alpha \qquad m_1 = 1,\ m_2 = \frac{x - x_c}{h_P},\ m_3 = \frac{y - y_c}{h_P},\ m_4 = \frac{z - z_c}{h_P}$$

◻ Projection of Strain

$$\int_E (\Pi_0^0 \nabla v_h) \cdot \mathbf{p}_0 \, d\mathbf{x} = \int_E \nabla v_h \cdot \mathbf{p}_0 \, d\mathbf{x} \quad \forall \mathbf{p}_0 \in [\mathcal{P}_0(E)]^2$$

$$\mathbf{p}_0 = \sum_{\alpha=1}^{n_{\mathbf{p}_0}} a_\alpha \mathbf{m}_\alpha \qquad \mathbf{m}_1 = \begin{bmatrix} 1 \\ 0 \\ 0 \end{bmatrix}, \mathbf{m}_2 = \begin{bmatrix} 0 \\ 1 \\ 0 \end{bmatrix}, \mathbf{m}_3 = \begin{bmatrix} 0 \\ 0 \\ 1 \end{bmatrix}$$

$$\int_E \Pi_0^0 (\nabla v_h) \cdot \mathbf{p}_0 \, d\mathbf{x} = \int_{\partial E} v_h \mathbf{p}_0 \, d\mathbf{x} - \int_E v_h \mathrm{div}(\mathbf{p}_0) \, d\mathbf{x}$$

Construction of Stiffness Matrix

Element Stiffness Matrix

$$\mathbf{K}_E = \mathbf{K}_{E,c} + \mathbf{K}_{E,s}$$

$$\mathbf{K}_{E,c} = \int_E \mathbf{B}^T \mathbf{C} \mathbf{B} \, d\mathbf{x}$$

$$\mathbf{B} = \sum_{\alpha=1}^{d} [\Pi_0^0 \nabla \boldsymbol{\phi}]_\alpha \otimes \bar{\mathbf{B}}_\alpha$$

$$\bar{\mathbf{B}}_1 = \begin{bmatrix} 1 & 0 \\ 0 & 0 \\ 0 & 1 \end{bmatrix}, \quad \bar{\mathbf{B}}_2 = \begin{bmatrix} 0 & 0 \\ 0 & 1 \\ 1 & 0 \end{bmatrix} \quad \text{for 2D}$$

$$\bar{\mathbf{B}}_1 = \begin{bmatrix} 1 & 0 & 0 \\ 0 & 0 & 0 \\ 0 & 0 & 0 \\ 0 & 1 & 0 \\ 0 & 0 & 0 \\ 0 & 0 & 1 \end{bmatrix}, \quad \bar{\mathbf{B}}_2 = \begin{bmatrix} 0 & 0 & 0 \\ 0 & 1 & 0 \\ 0 & 0 & 0 \\ 1 & 0 & 0 \\ 0 & 0 & 1 \\ 0 & 0 & 0 \end{bmatrix}, \quad \bar{\mathbf{B}}_3 = \begin{bmatrix} 0 & 0 & 0 \\ 0 & 0 & 0 \\ 0 & 0 & 1 \\ 0 & 0 & 0 \\ 0 & 1 & 0 \\ 1 & 0 & 0 \end{bmatrix} \quad \text{for 3D}$$

$$\mathbf{K}_{E,s} = \bar{\mathbf{K}}_{E,s} \otimes \mathbf{I}_d$$

$$\bar{\mathbf{K}}_{E,s} = (\mathbf{I}_n - \mathbf{P}_1^0)^T \boldsymbol{\Lambda} (\mathbf{I}_n - \mathbf{P}_1^0)$$

K. Park, H. Chi, and G.H. Paulino, 2020, Numerical recipes on virtual element method for elasto-dynamic explicit time integration, International Journal for Numerical Methods in Engineering 121, 1-31

VEM vs FEM

Macro Elastic Modulus

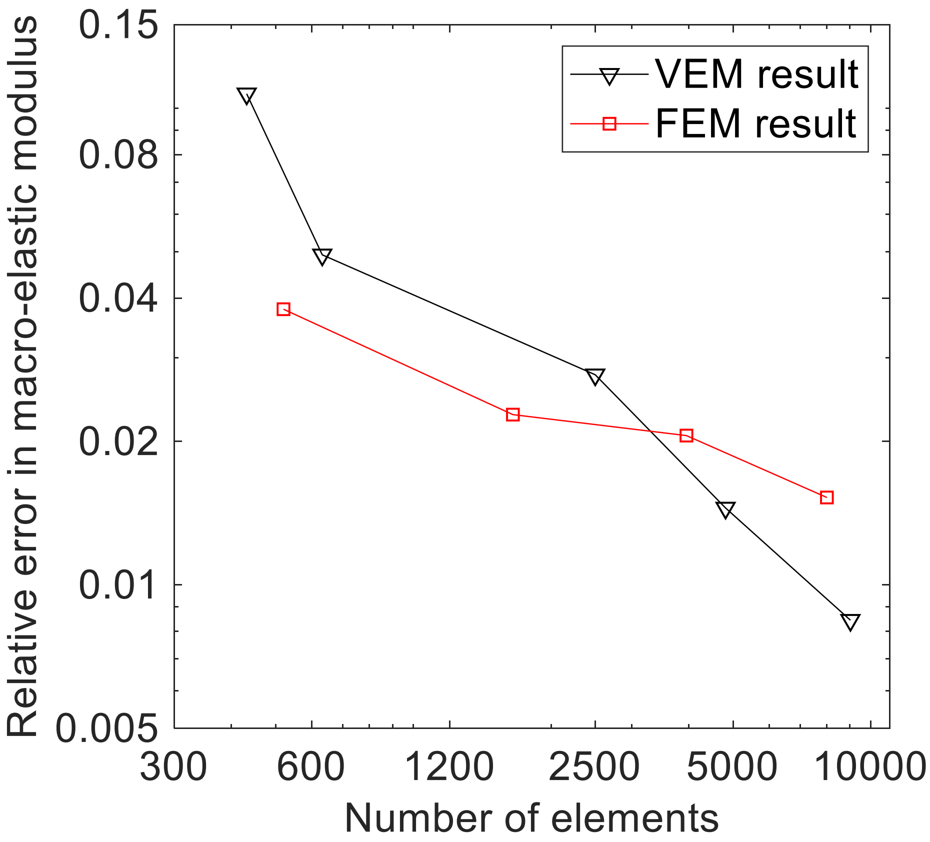

Total Strain Energy

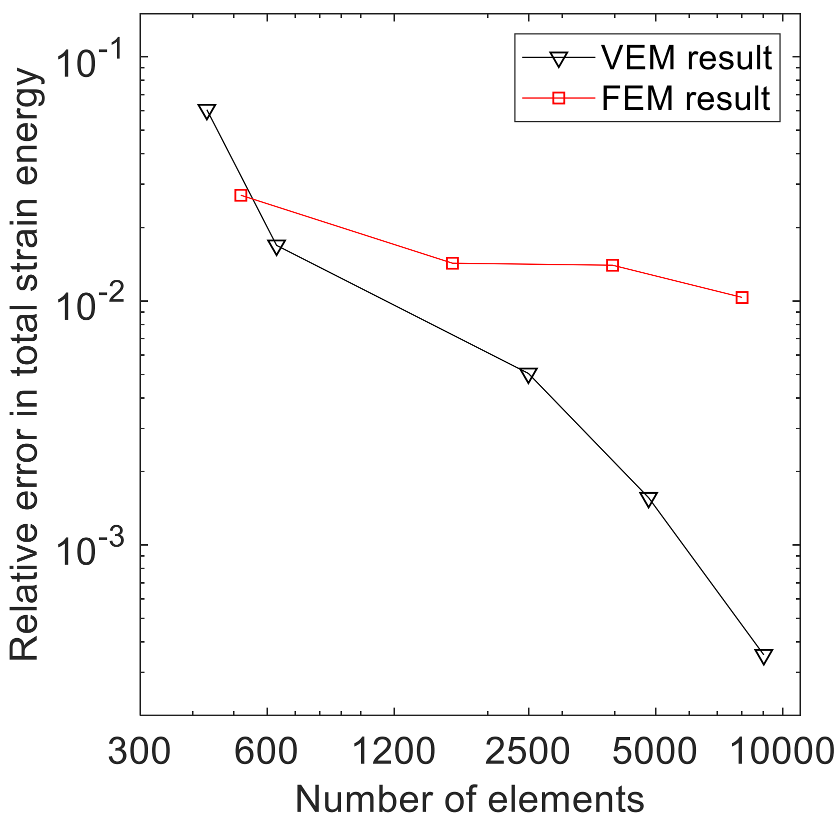

Material Properties

Young's Modulus

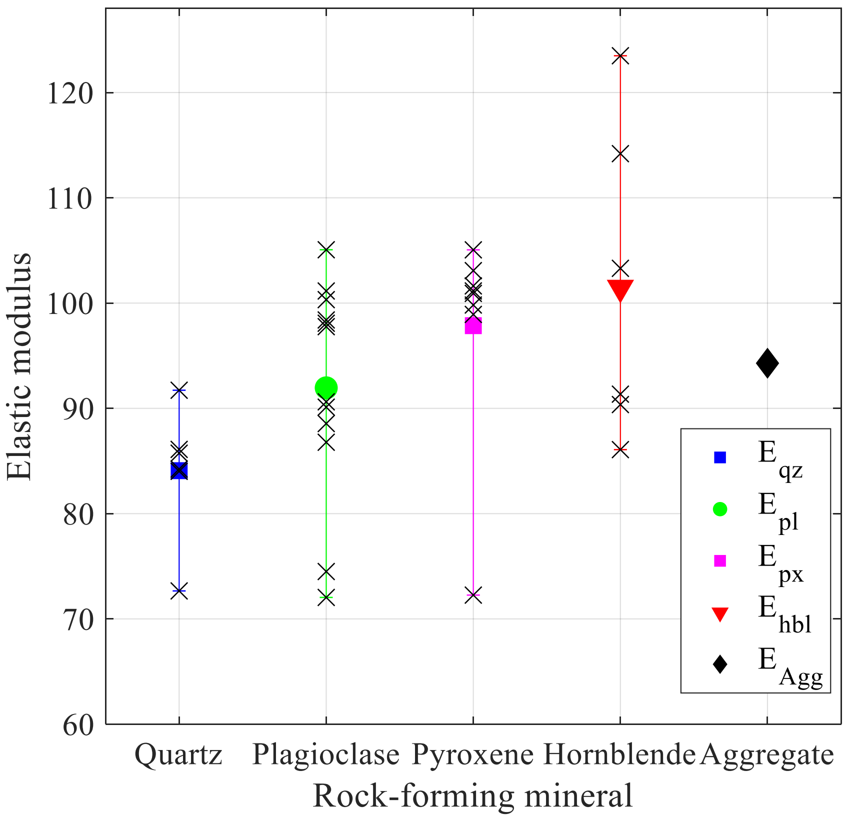

Poisson's Ratio

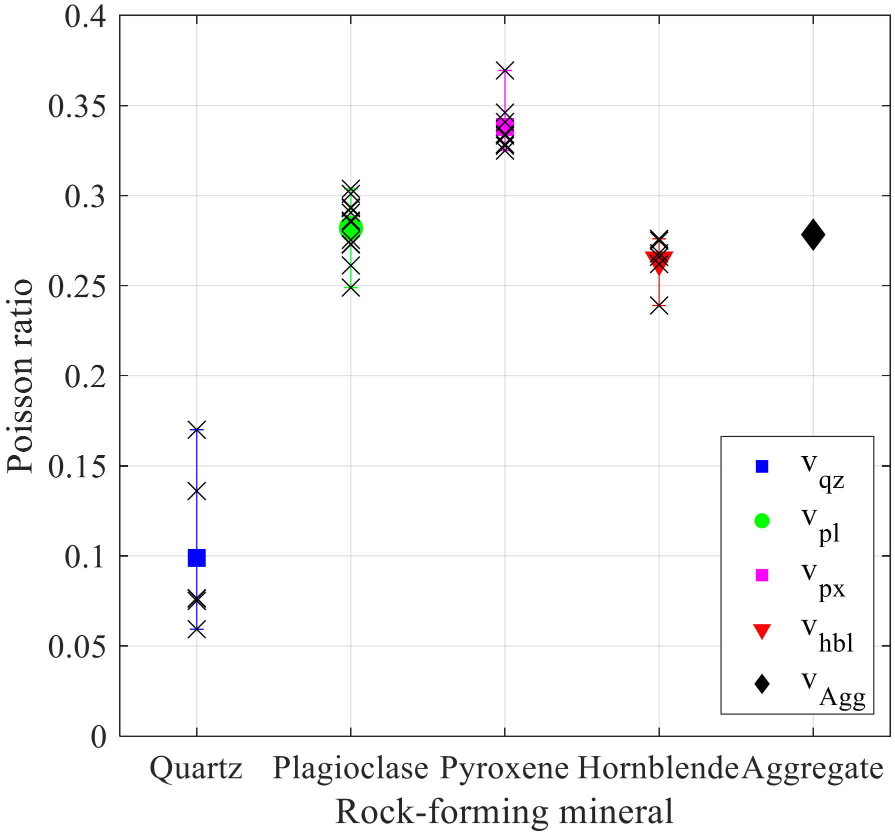

Result

Concrete volume change

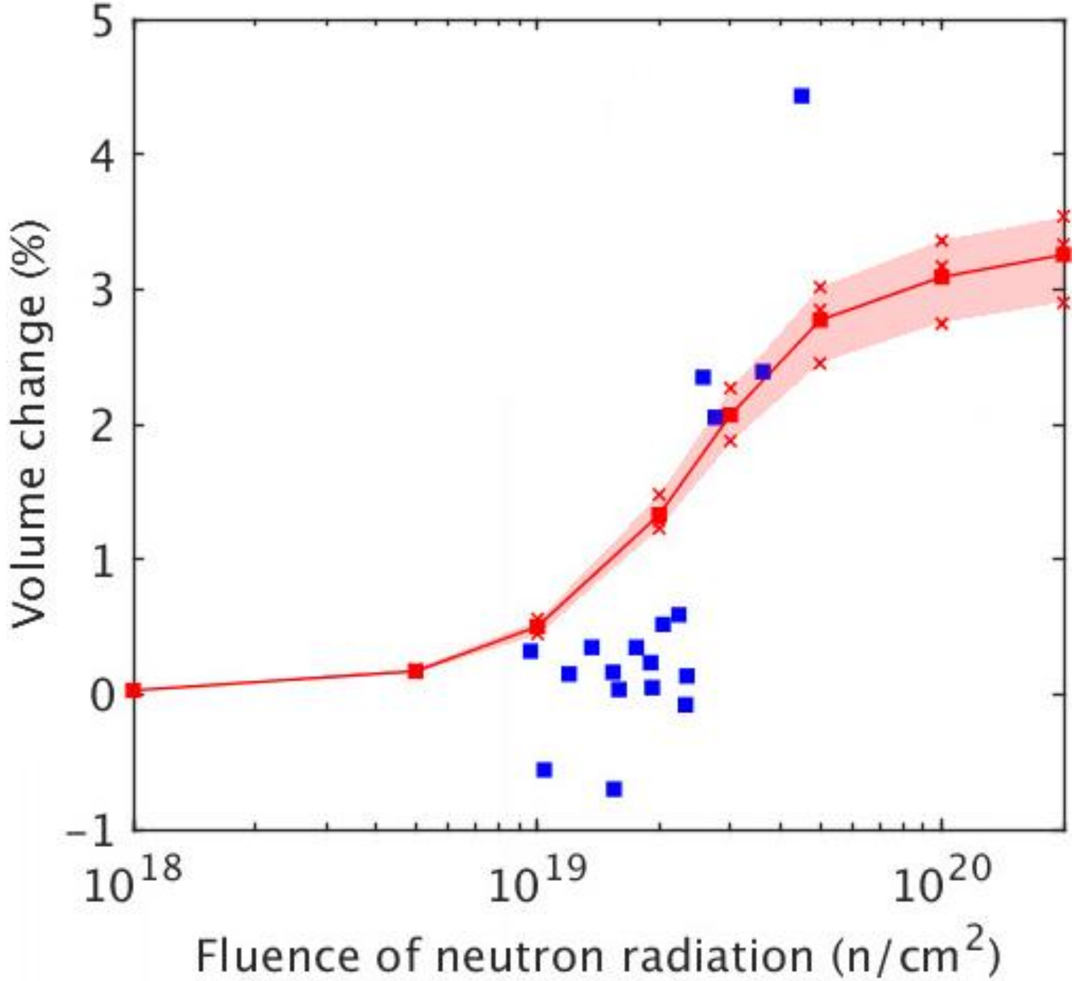

$$Volume\ change = \left|\frac{V - V_0}{V_0}\right|$$

$$V = \sum_{i=1}^{Nelem} A_i t$$

$$V_0 = \sum_{i=1}^{Nelem} A_{0,i} t$$

Result

Concrete volume change

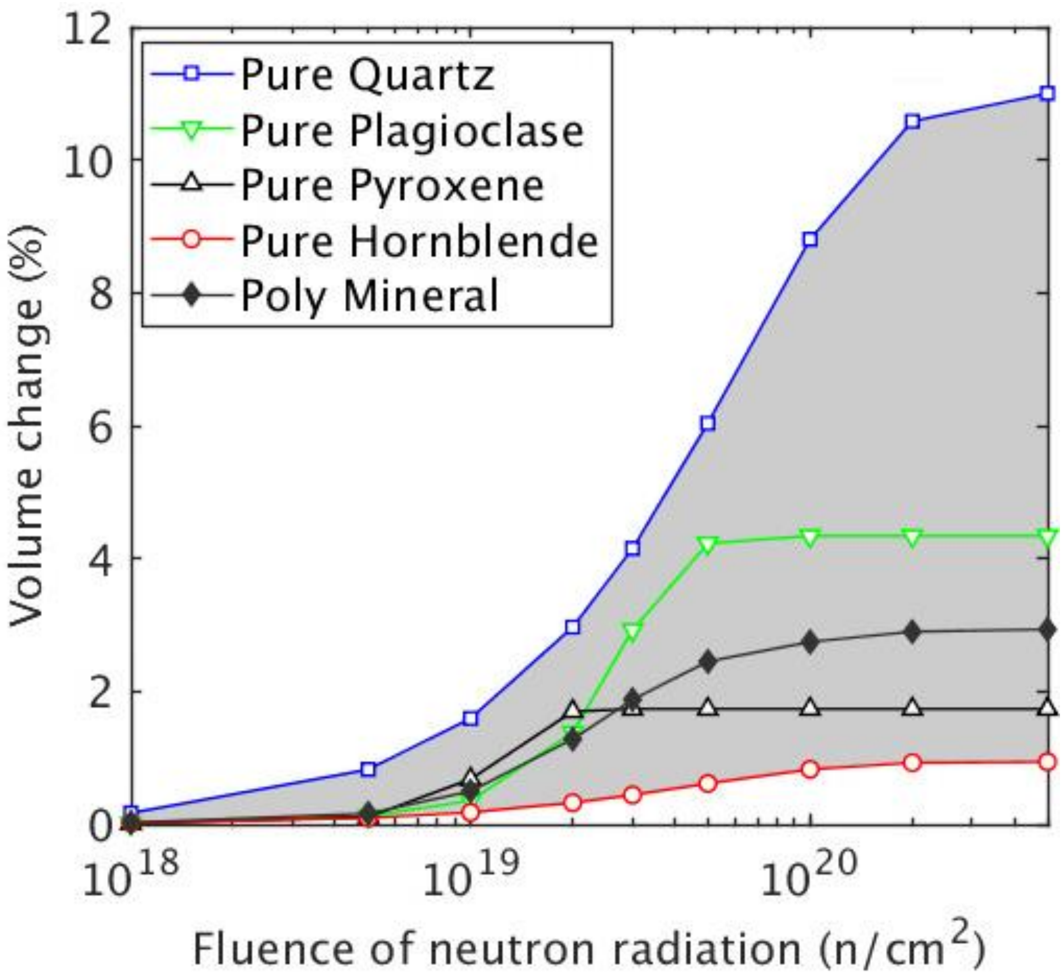

Poly Mineral Aggregate

Pure Quartz Aggregate

Pure Plagioclase Aggregate

Pure Pyroxene Aggregate

Pure Hornblende Aggregate

[1] Le Pape, Y., Giorla, A., & Sanahuja, J. (2016). Combined effects of temperature and irradiation on concrete damage. *Journal of Advanced Concrete Technology*, *14*(3), 70-86.

Numerical Examples

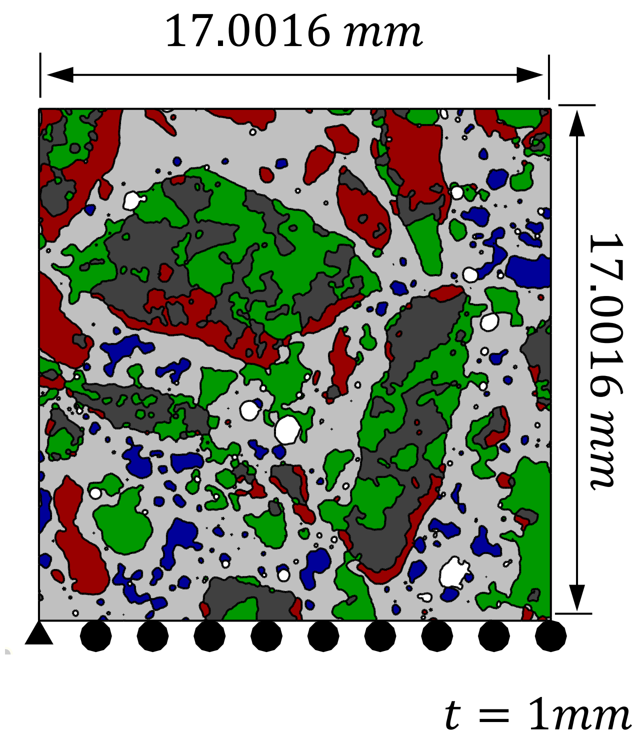

Domain size : 1232 x 1232 pixels

Temperature : 25, 100, 200

Radiation : $10^{18} \sim 2 \times 10^{21}\ n/cm^2$

Plane strain condition

Initial strain : $\boldsymbol{\varepsilon}_{\boldsymbol{in}} = [\varepsilon_V/2 \quad \varepsilon_V/2 \quad 0]^T$

	석영(Qz)	사장석(Pl)	휘석(Px)	각람석(hbl)	페이스트 (Paste)
E(MPa)	94.73	94.90	88.94	141.14	20.00
ν	0.0869	0.2786	0.3489	0.2424	0.2000

Radiation Induced Volume Expansion

Fitting equation : Zubov and Ivanov'S sigmoidal model with linear temperature… [1]

$$\varepsilon_V(\Phi, T) = \varepsilon_{max} \frac{1 - e^{-\frac{\Phi}{\Phi_c}}}{1 + e^{-\frac{\Phi - \Phi_L}{\Phi_c}}}$$

characteristic fluence [Φ_c , n/pm^2]
Latency fluence [Φ_L, n/pm^2]

$$\Phi_i = a_i T + b_i$$

	Quartz	Plagioclase	Pyroxenes	Hornblendes
$\varepsilon_{max}(\%)$	17.8	7.0	2.8	1.5

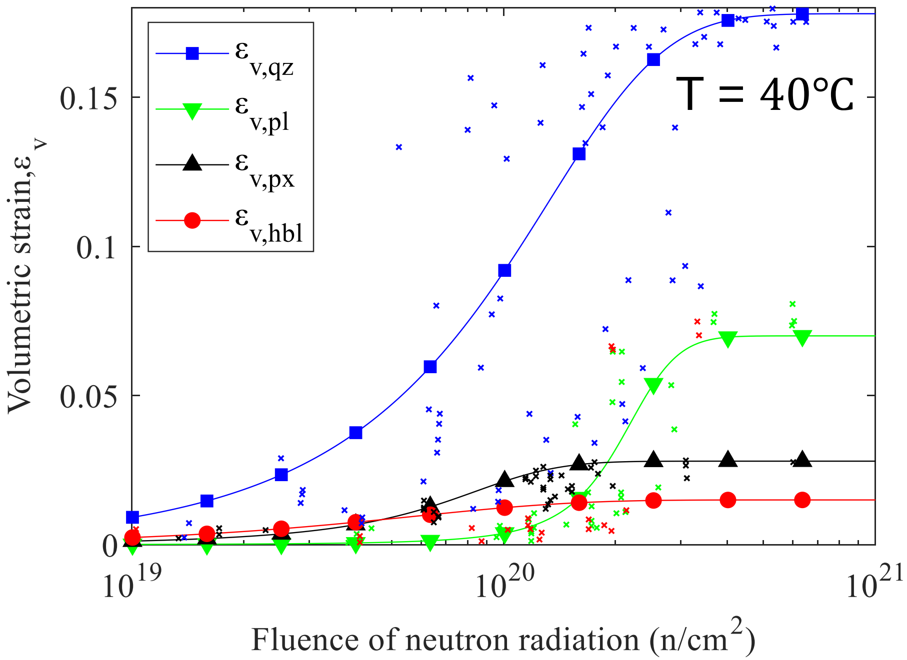

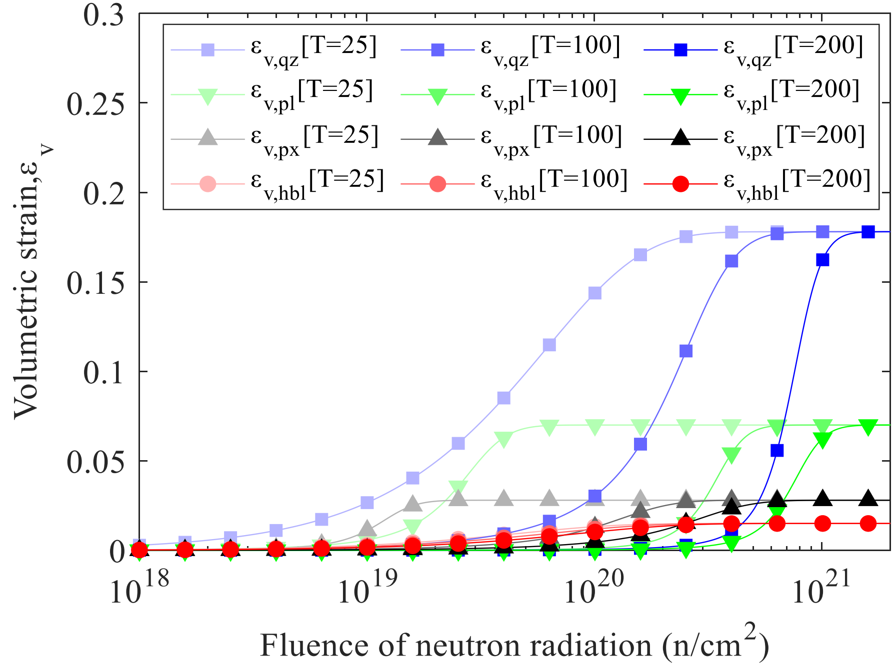

[1] Le Pape, Y., Alsaid, M. H., & Giorla, A. B. (2018). Rock-forming minerals radiation-induced volumetric expansion–revisiting literature data. Journal of Advanced Concrete Technology, 16(5), 191-209.

Result : Concrete Volume Change

Concrete volume change

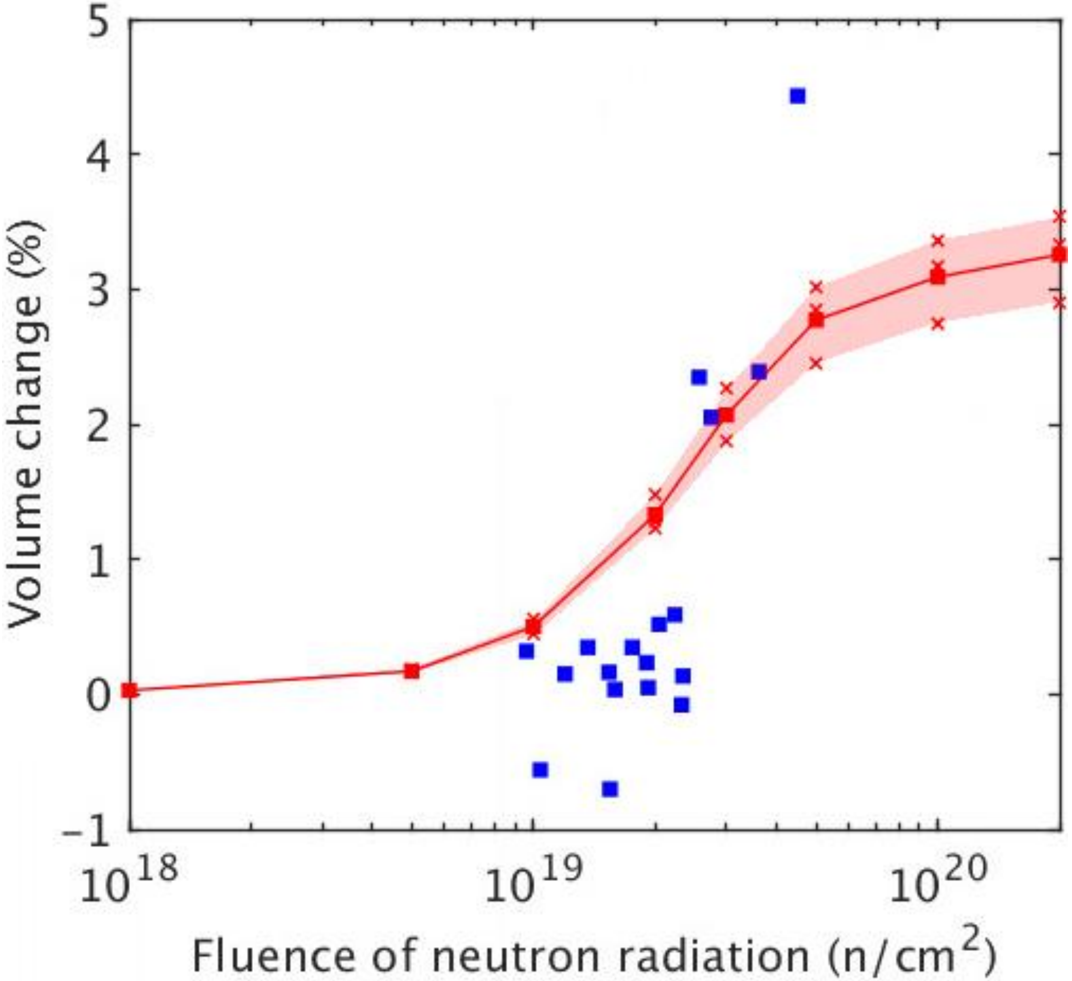

H = 10, 40, 70

Temperature = 25

Poly mineral Aggregate

$$Volume\ change = \left|\frac{V - V_0}{V_0}\right|$$

$$V = \sum_{i=1}^{Nelem} A_i t$$

$$V_0 = \sum_{i=1}^{Nelem} V_{0,i} t$$

Result : Effects on the Temperature

Concrete volume change

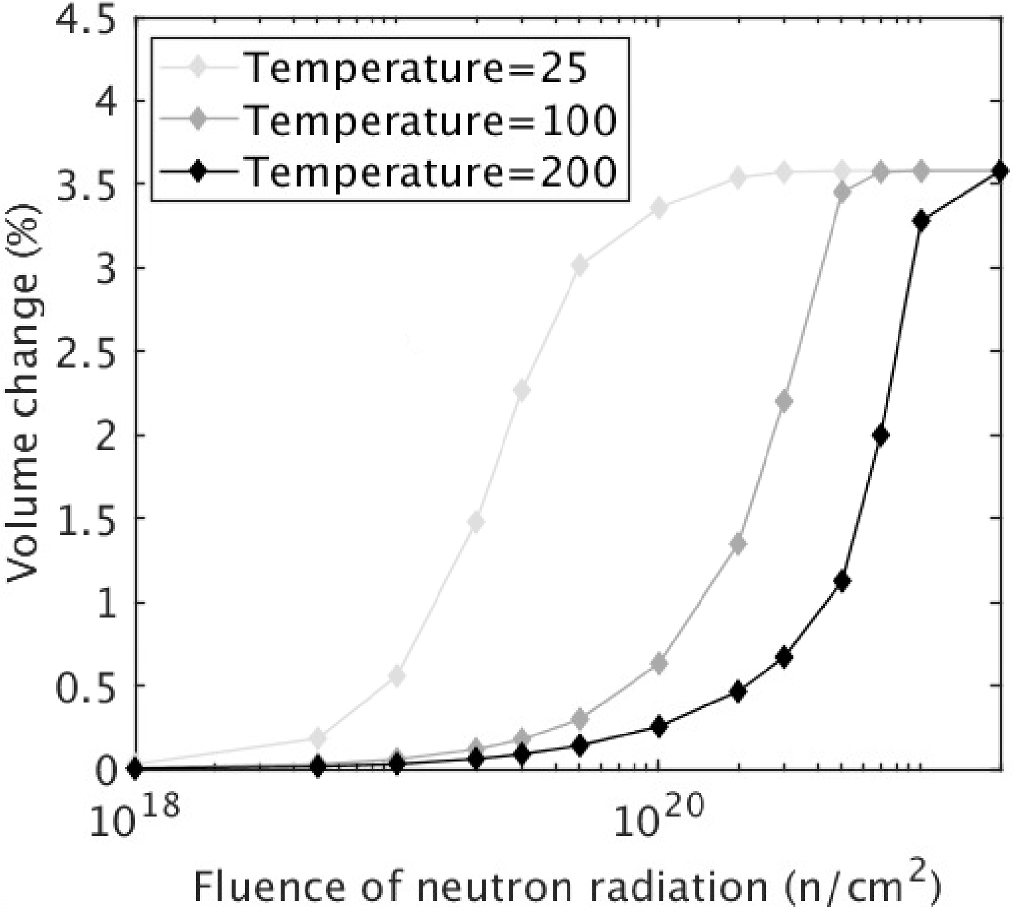

H = 40

Temperature = 25, 100, 200

Poly mineral Aggregate

[1] Le Pape, Y., Giorla, A., & Sanahuja, J. (2016). Combined effects of temperature and irradiation on concrete damage. *Journal of Advanced Concrete Technology*, *14*(3), 70-86.

Result : Effects on the Mineral Component

Concrete volume change

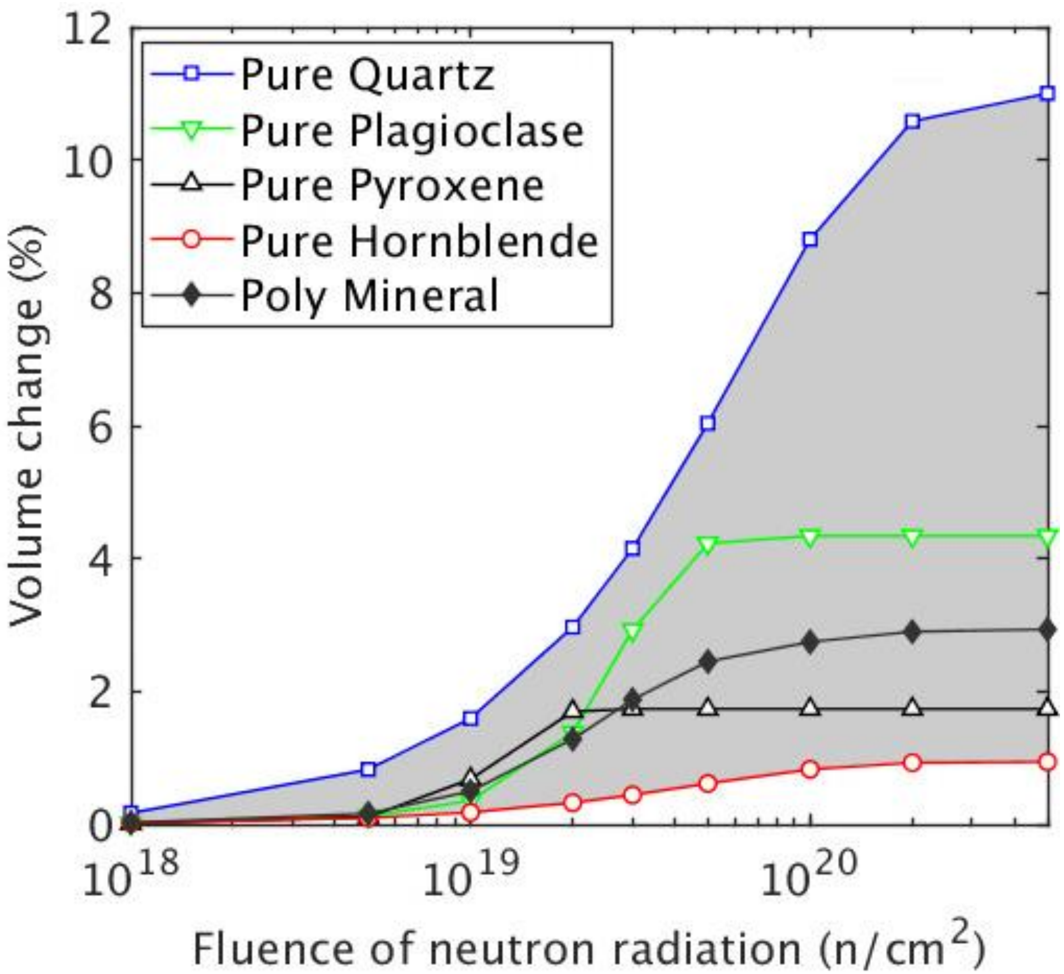

H = 40

Temperature = 25

Poly Mineral Aggregate

Pure Quartz Aggregate

Pure Plagioclase Aggregate

Pure Pyroxene Aggregate

Pure Hornblende Aggregate

[1] Le Pape, Y., Giorla, A., & Sanahuja, J. (2016). Combined effects of temperature and irradiation on concrete damage. *Journal of Advanced Concrete Technology*, *14*(3), 70-86.

Result : Effects on the homogenization

Maximum principal strain (Scale factor = 5)

H = 40 , Temperature = 25 , Radiation = $5 \times 10^{20}\ n/cm^2$

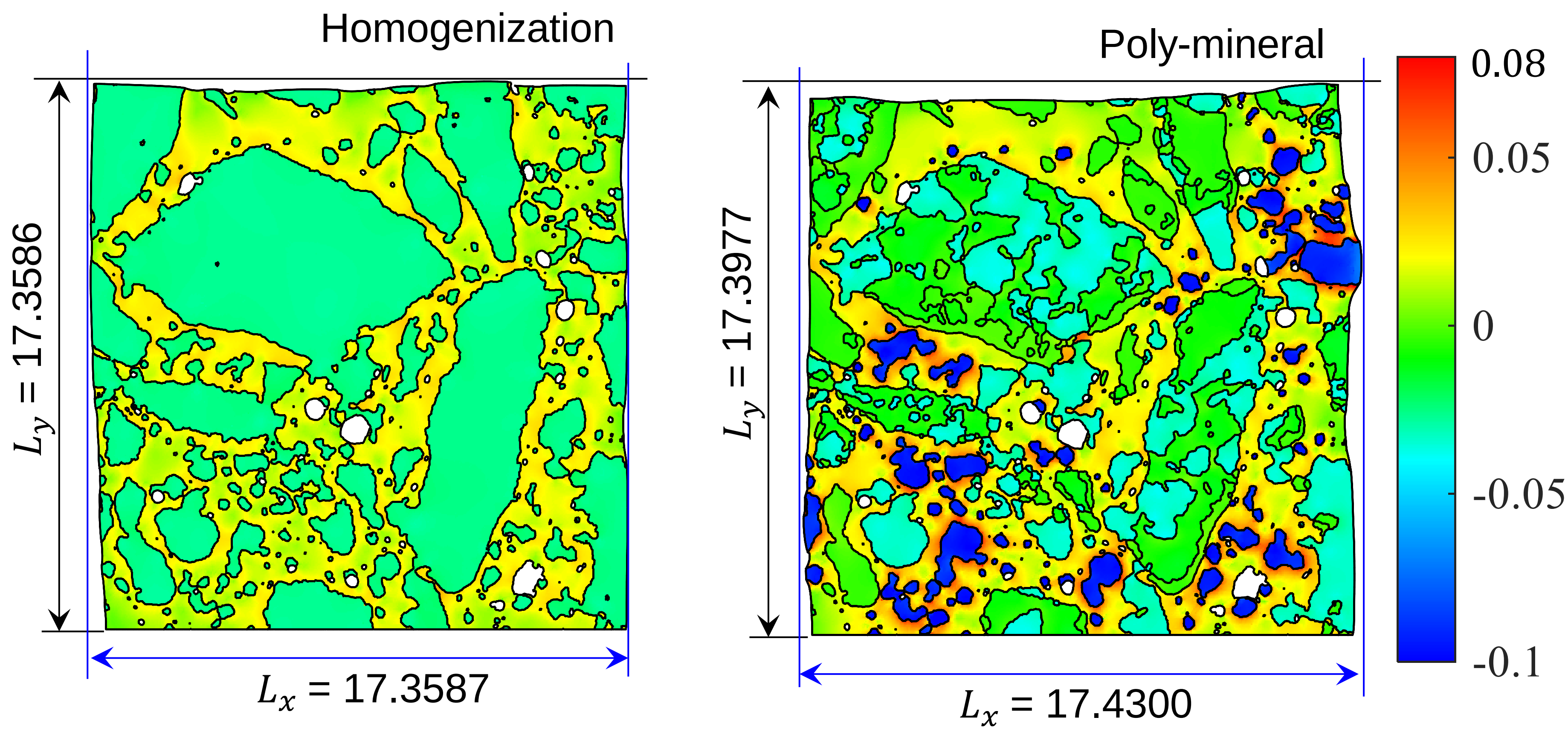

$\varepsilon_1 = -0.0291{\sim}0.0517$ $\varepsilon_1 = -0.1124{\sim}0.1075$

Result : Effects on the homogenization

Concrete volume change H = 40 , Temperature = 25

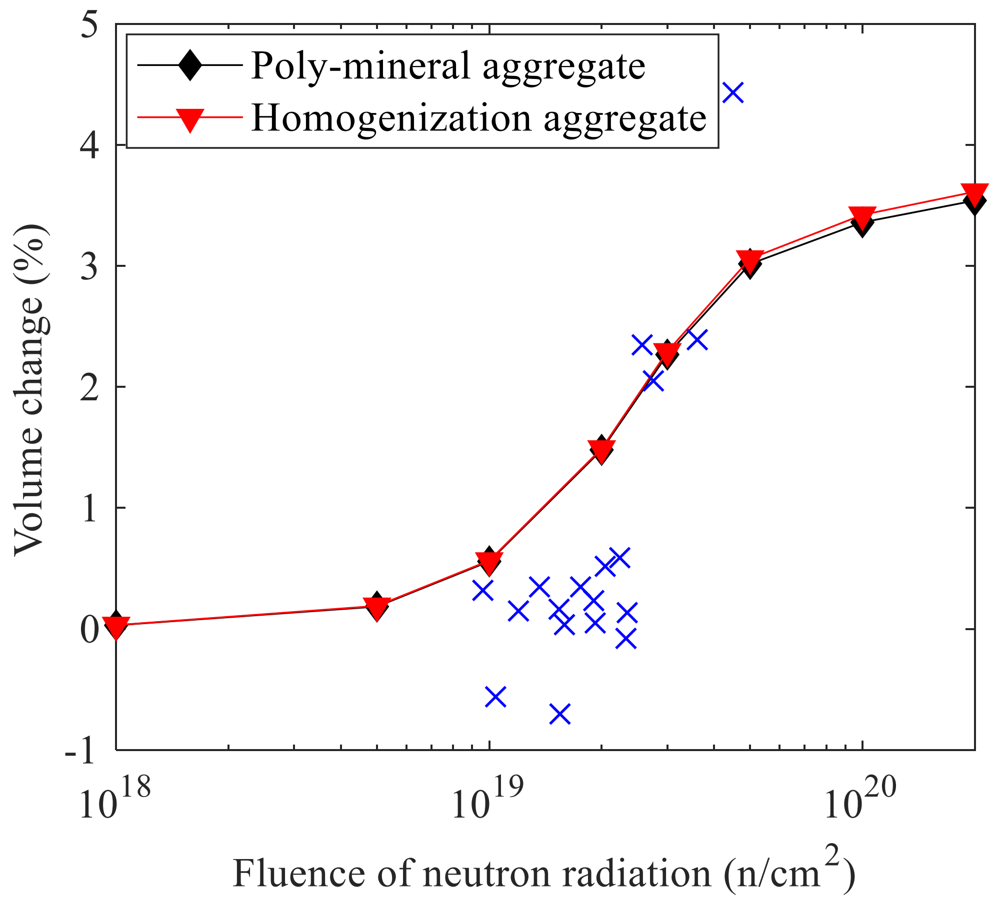

$$\text{Volume change} = \frac{\sum_i A_i}{\sum_i A_{0,i}} - 1$$